B. THE PHYSICS OF IMPACT AND DEFORMATION: MULTIPLE IMPACT

VII. The erosion of solids by the repeated impact of liquid drops

By N. L. Hancox† and J. H. Brunton

Surface Physics, Cavendish Laboratory, University of Cambridge

[Plates 16 to 21]

An investigation of the erosion of solids by repeated liquid impact at relatively low velocities has been carried out. The work has shown that even at low velocities compressible behaviour of the liquid is important in determining the impact pressure. An attempt has also been made to determine the distribution of the impact load. The mechanism of erosion in brittle polymers and in ductile metals has been studied. The effect of altering the conditions of impact on the erosion behaviour is described.

Introduction

In this paper we report on an investigation we have made into the mechanism of erosion damage in solids arising from the impact of liquid drops at relatively low speeds. An attempt has been made to analyse the impact forces and to examine the effect of these forces on the deformation process. In ductile metals yielding was found to begin locally at average impact pressures appreciably below the average flow stress for the metal. The regions which yielded initially were further deformed and pitted by the liquid flow. In brittle materials erosion was preceded by Hertzian fractures along the boundary of the impact area. Erosion itself—that is removal of material from the surface—was caused by impingement of the liquid flow against the edges of the surface fractures. The effect of altering the erosion conditions and the properties of the solid on these processes has been investigated.

Previous studies of erosion

The erosion problem has been familiar to engineers for the last 50 years or so and during this time a great deal has been written about it. We shall trace only very briefly some of the advances which have been made. More detailed accounts are to be found in reviews of the subject (see, for example, Engel 1957, A.S.T.M. 1961).

One of the earliest experimental studies was started in 1925 at the Parson's steam turbine plant; this showed conclusively that erosion was caused by water drops carried by the steam into the path of the rotating blades (Parsons 1936). Flow diagrams of this process have been given by Gardner (1932) and Mochel (1950). Hardness was generally found to be the property which to a large extent determined erosion resistance (Honegger 1927; Gardner 1932; de Haller 1933, 1940). Chemical attack was discounted as a prime cause of failure. It was found that the rate of erosion varied markedly with impact velocity. Experimental values showed erosion increasing as the third, fourth and even higher powers

† Present address: Department of Reactor Physics, University of Birmingham.

of velocity (de Haller 1933; Vater 1937; Beal & Wahl 1951; Fyall, King & Strain 1956, 1957). In some materials a critical velocity was found below which erosion was not detected. De Haller (1933) found that the minimum velocity to cause erosion decreased as the drop size increased. He also observed that the smaller the area of the specimen struck the greater the apparent resistance to damage. Von Schwarz & Mantel (1936) examined the microstructure of eroded brass specimens and noted that after they lost their original polish the surfaces became pitted with small depressions.

One of the first studies of the pressure developed during a liquid drop impact was made by Cook (1928). He drew attention to the fact that high impact pressures could arise as a result of the water-hammer effect in the liquid. Cook expressed the impact pressure P as

$$P = V\sqrt{(\rho/\beta)}, \tag{1}$$

where V is the impact velocity, ρ the liquid density and β its compressibility. The water hammer pressure is generally greater than the steady flow pressure and in fact is only limited by the compressibilities of the liquid and the solid against which it strikes.

Equation (1) can be rewritten in terms of the velocity of the compression wave C in the liquid

$$P = \rho CV. \tag{2}$$

If the compressible deformation of the solid impact surface is taken into account, the expression for the impact pressure becomes

$$P = \rho CV\left[\frac{\rho_s C_s}{\rho_s C_s + \rho C}\right], \tag{3}$$

where ρ_s and C_s are the density and compression wave velocity in the solid. The relation given in (3) was used by De Haller (1933) in his study of erosion under liquid impact. Experimental verification of this basic equation has been provided by Engel (1955) and Bowden & Brunton (1961).

Recent work has been mainly concerned with a study of single impact (Engel 1955, 1958, 1959; Jenkins & Booker 1958*a*, *b*). Some of the results of this work, particularly on the breakup of the liquid drop, are applicable to the more complex problems which occur under conditions of repeated impact.

Experimental

Specimens were eroded using a small wheel and jet apparatus (figure 1). A 20·3 cm diameter wheel was driven by a 1·25 h.p. electric motor at 9000 rev/min such that a specimen screwed into the rim of the wheel cut through, once per revolution, a single continuous jet of liquid flowing parallel to the axis of rotation. The frequency of rotation of the wheel was measured by a phototransistor pickup. The diameters of the jets varied between 0·4 and 2·6 mm. For most of the experiments filtered mains water from a constant pressure head was used to form the jet.

The specimens were machined into bars 3 cm long and 3·2 mm square, with one end of the bar threaded. In cases where machining was undesirable, specimens were mounted in specimen holders and the holder attached to the disk.

For the early stages of erosion the usual weight loss method of measuring damage could not be used. Instead sensitive instruments were used to detect and measure slight changes

in the surface deformation. In some cases the amount of light reflected from the eroded region was measured by a photomultiplier tube mounted in a microscope eyepiece and the reading compared with the light reflected from a polished undamaged region of the same specimen. The ratio of the two readings was taken as a measure of the deformation. The method was capable of great sensitivity, especially when detecting the first small depressions which appeared in the surface at the start of the erosion process.

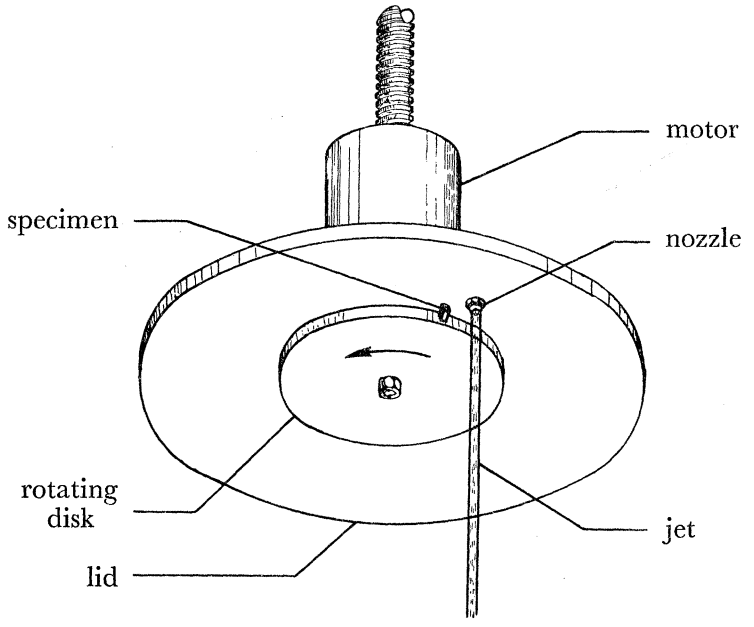

FIGURE 1. Principle of the wheel and jet method for producing erosion.

A second method for measuring deformation involved the use of a Talysurf profilometer. This is a stylus instrument which records the surface contours at magnifications up to 40000. The mean deviation of the eroded surface from the original polished level was taken as a measure of the erosion damage.

THE IMPACT FORCE

The flow of a liquid drop on impact, or, as in the present experiment of a liquid cylinder struck from the side by a rigid surface is highly complex and cannot be easily analysed. The problem can, however, be made simpler by considering only the very early stages of impact before appreciable flow of the liquid occurs. In this way we can examine the magnitude and distribution of the impact forces and investigate the extent to which they account for the observed erosion damage.

Consider a liquid cylinder being struck by a plane rigid surface as shown in figure 2. Contact occurs first along a line OL. As the collision progresses the line becomes a plane of contact ABCD. Initially, the sides of this plane AD and BC will move outwards from the centre at a speed greater than that of the compression waves set up at the interface of the solid and the liquid. This fact, which was pointed out by Field (1962), arises from the geometry of the system. The significance of this is that liquid in contact with the area ABCD is compressibly deformed, while the remainder of the liquid surface outside ABCD

is unaware of the impact (since the stress waves have not yet arrived) and therefore sideways flow does not occur. Eventually at some short distance from the centre line (the distance depending upon the impact velocity), the velocity of the sideways movement of the boundaries AD and BC becomes less than the compression wave velocity. At this stage flow is possible and the pressure is relieved in the central compressed zone.

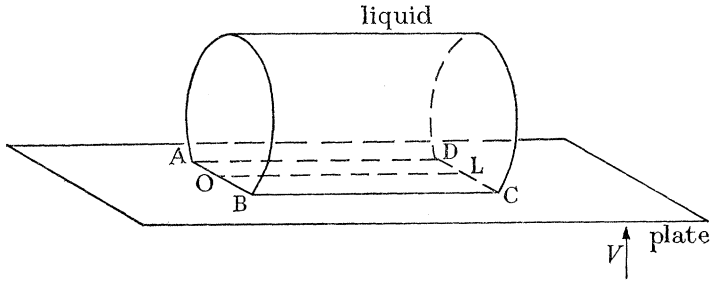

FIGURE 2. Plane solid surface striking a compressible liquid cylinder.

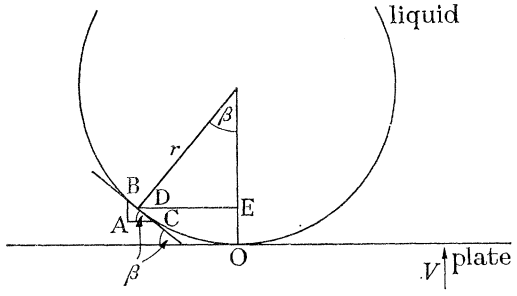

FIGURE 3. Cross section through liquid cylinder and plate.

The limit of compressible deformation of the liquid may be obtained as follows: figure 3 represents a liquid cylinder and an impact plate in section. For a compression wave outside the area of contact, a wave initiated at C must arrive at a nearby point B before the plate reaches B. Thus, if the plate velocity is V, then for a stress wave to move ahead of the plate we must have

$$V/C < \sin \beta, \tag{4}$$

where β is the liquid/solid interface angle and C the speed of the compression wave. The limit of compressible deformation of the drop is given by

$$V/C = \sin \beta, \tag{5}$$

while the corresponding maximum width of the area of contact (AB, figure 2) is

$$2r \sin \beta = 2rV/C, \tag{6}$$

where r is the radius of the cylinder. Inside this width of contact the pressure P exerted on the striking surface, assuming this to be rigid, is given by the water-hammer equation

$$P = \rho CV, \tag{7}$$

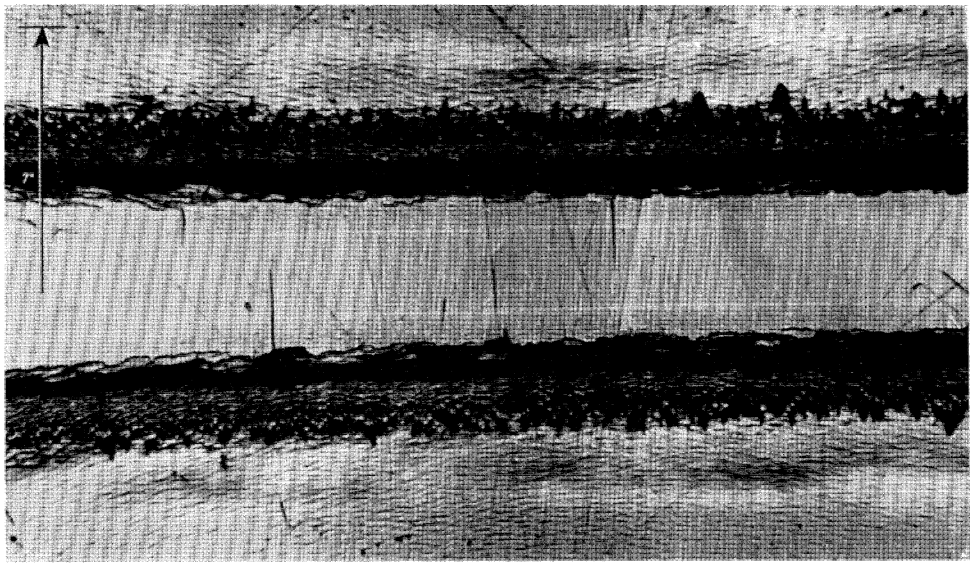

FIGURE 4. Deformation of a polymethylmethacrylate specimen which has been shot through a 1 mm diameter jet of mercury at 150 m/s. The radius of the jet is shown by the arrow. The photograph was taken with reflected light.

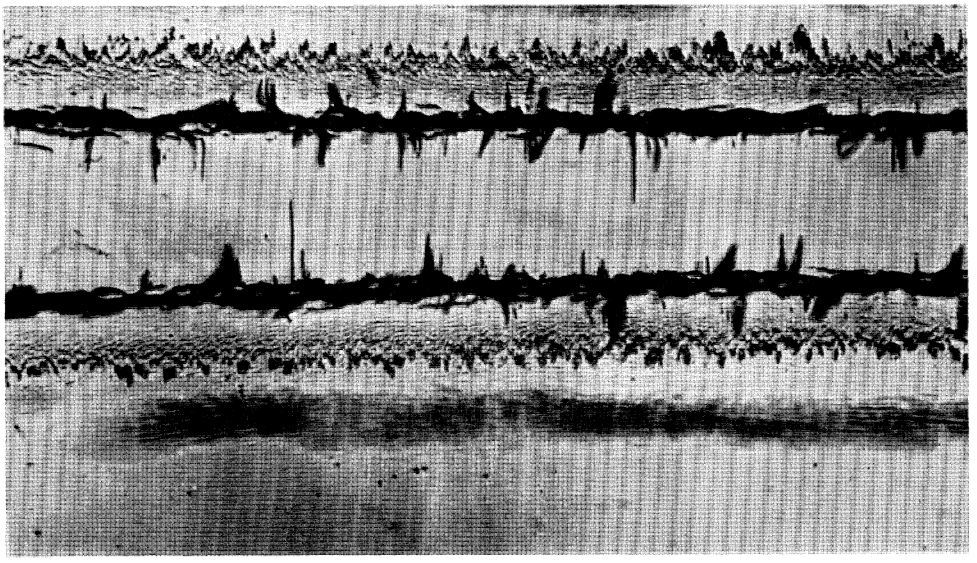

FIGURE 5. The same area as that shown in figure 4 but now photographed in transmitted light.

(*Facing p.* 124)

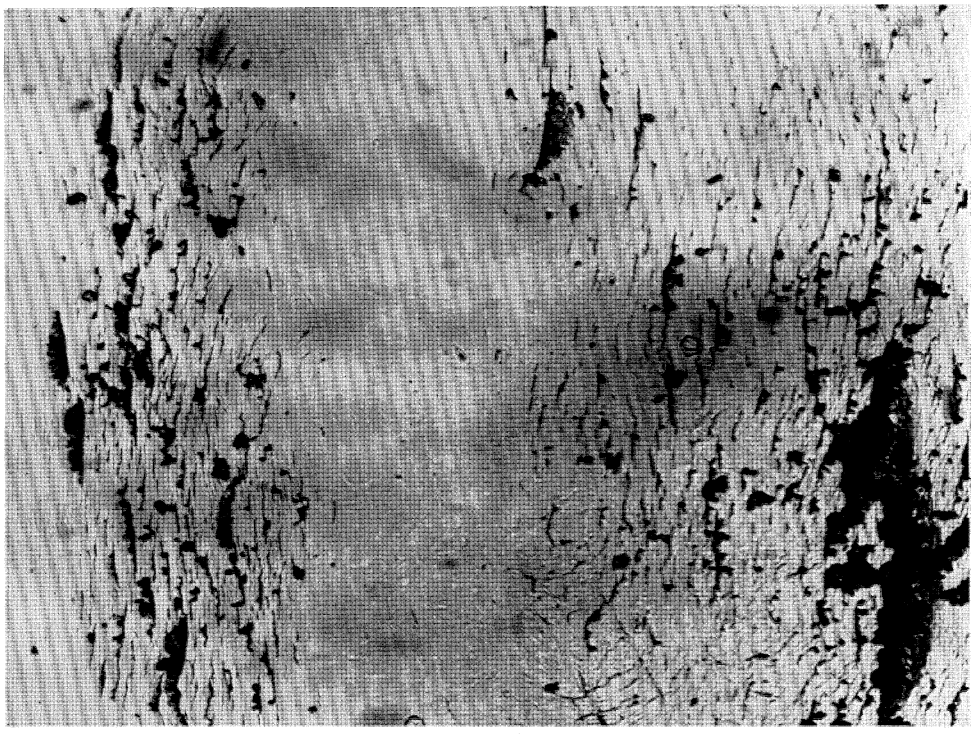

FIGURE 8. Fractures in a polymethylmethacrylate specimen after 3500 impacts at 68 m/s. The bands of fracture lie parallel to the jet axis.

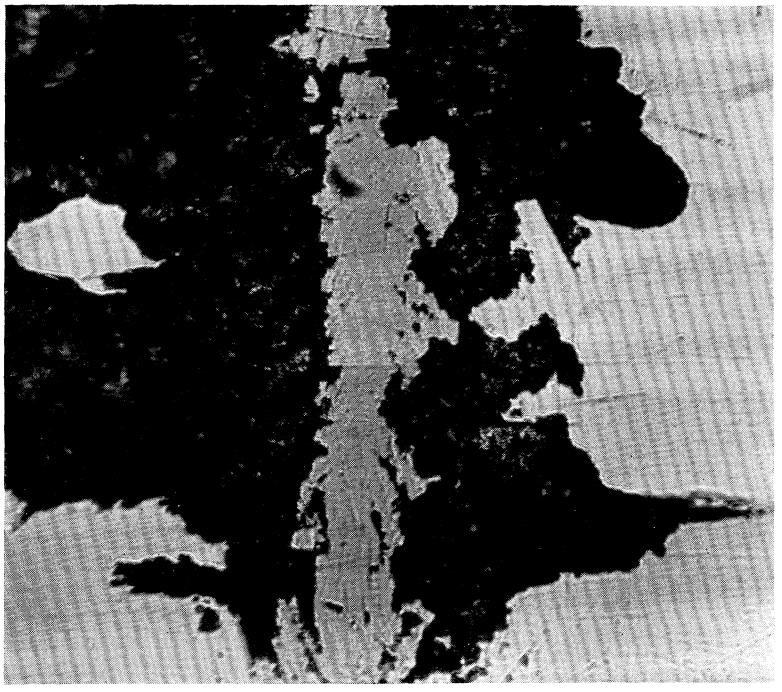

FIGURE 9. The surface of a heavily eroded polymethylmethacrylate specimen which has received 47 000 impacts at a velocity of 67 m/s. The central region is only lightly fractured at this stage.

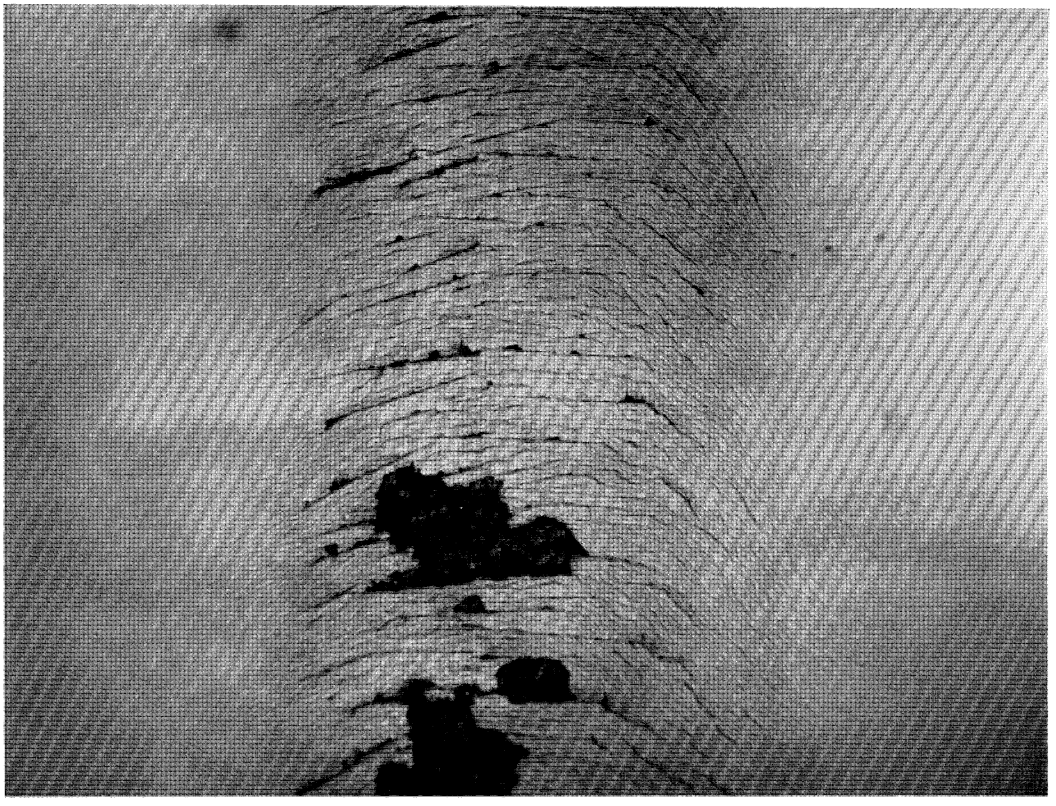

FIGURE 10. Fractures in a polymethylmethacrylate specimen eroded such that the impact surface was tilted at an angle of 9° to the jet axis. The area shown in the lower half of the photograph struck the jet first. (Magn. × 33.)

FIGURE 14. A small depression in copper. Depressions similar to this provide the first detectable signs of permanent deformation. The specimen illustrated has received 8000 impacts at 51 m/s. (Magn. × 500.) Phase contrast photograph.

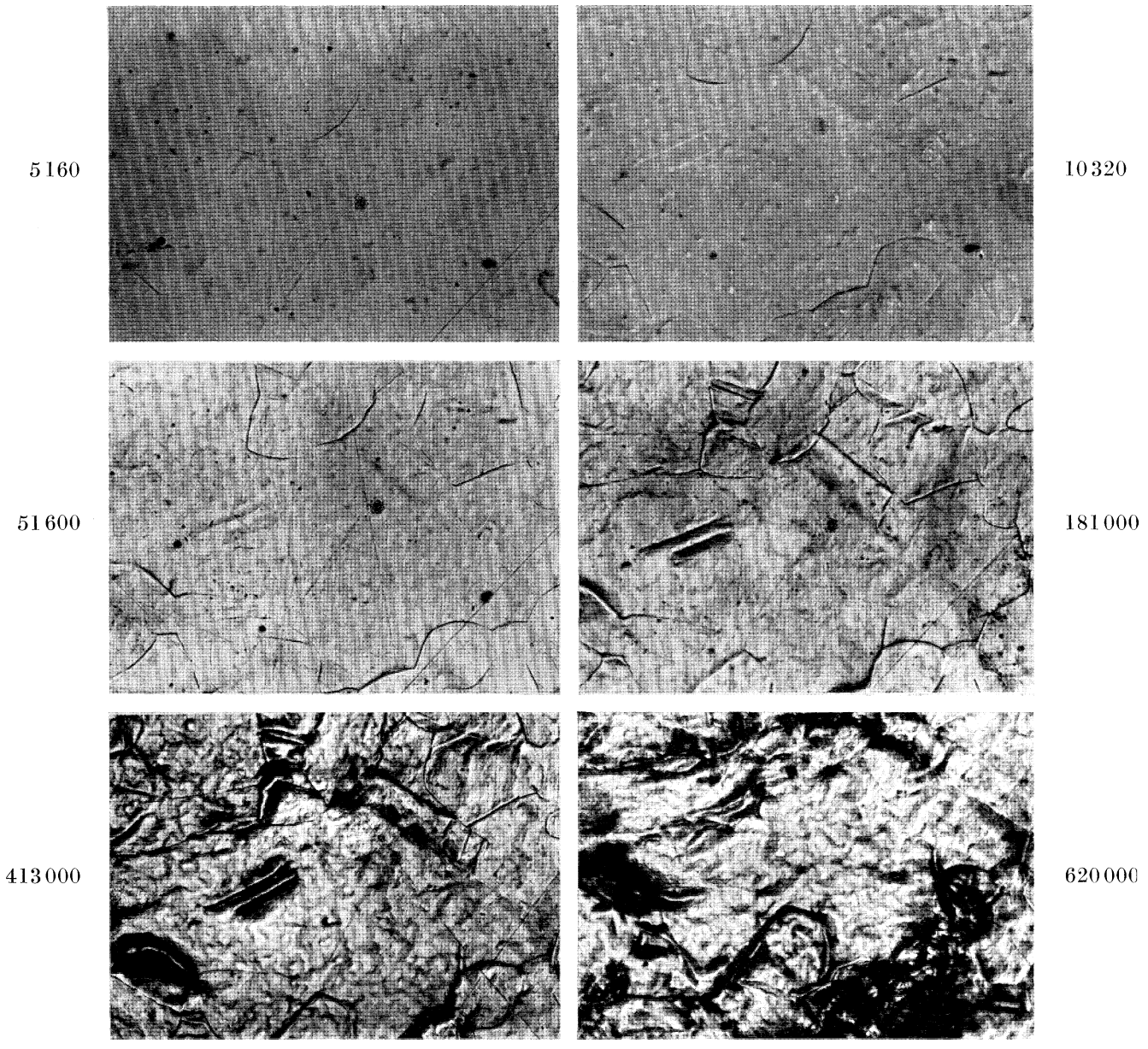

FIGURE 15. The development of erosion damage in copper. The number of impacts is shown besides each frame. The impact velocity was 52 m/s and the water jet diameter 1·35 mm. (Magn. × 190.)

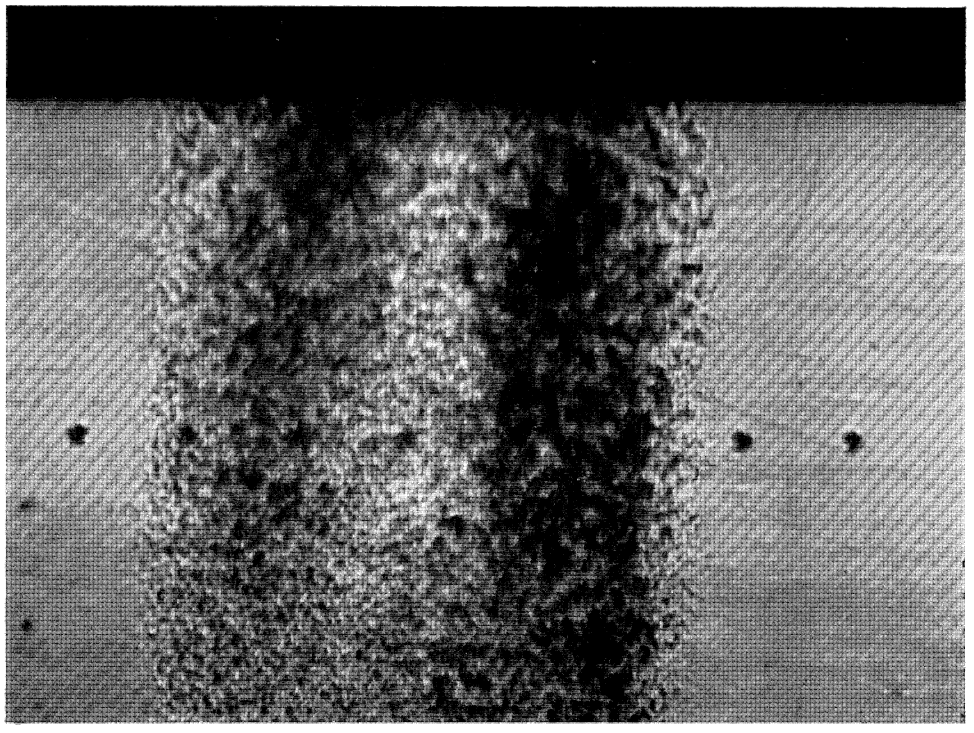

FIGURE 19. Two bands of deformation in a specimen of low carbon steel. The bands run parallel to and lie on either side of the centre line of impact. (Magn. × 35.)

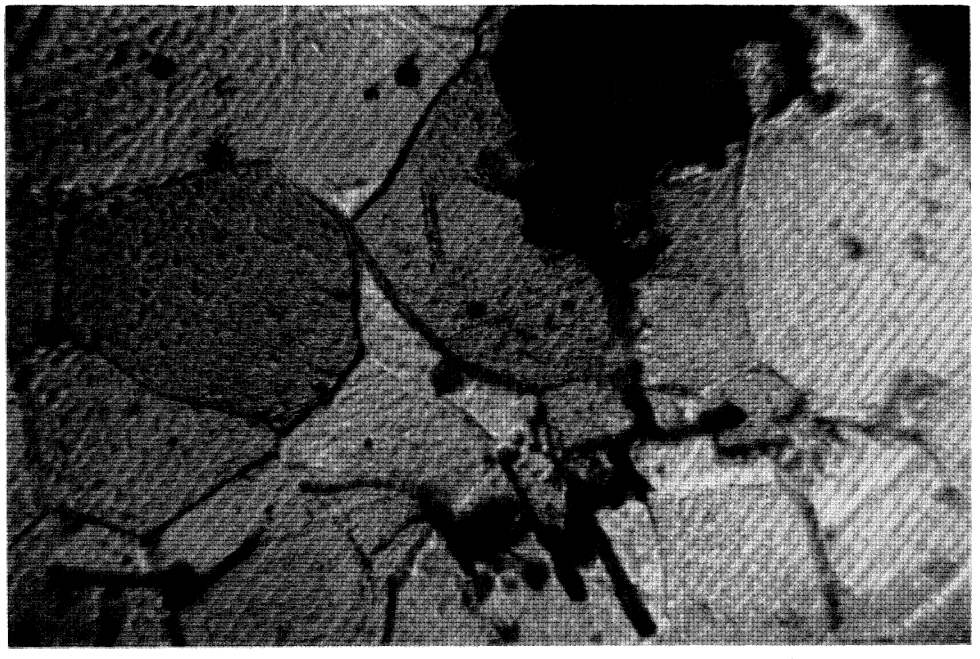

FIGURE 20. A crack spreading from the root of a surface pit in an eroded, sectioned and etched specimen of low carbon steel. 10^6 impacts at 90 m/s. (Magn. × 900.)

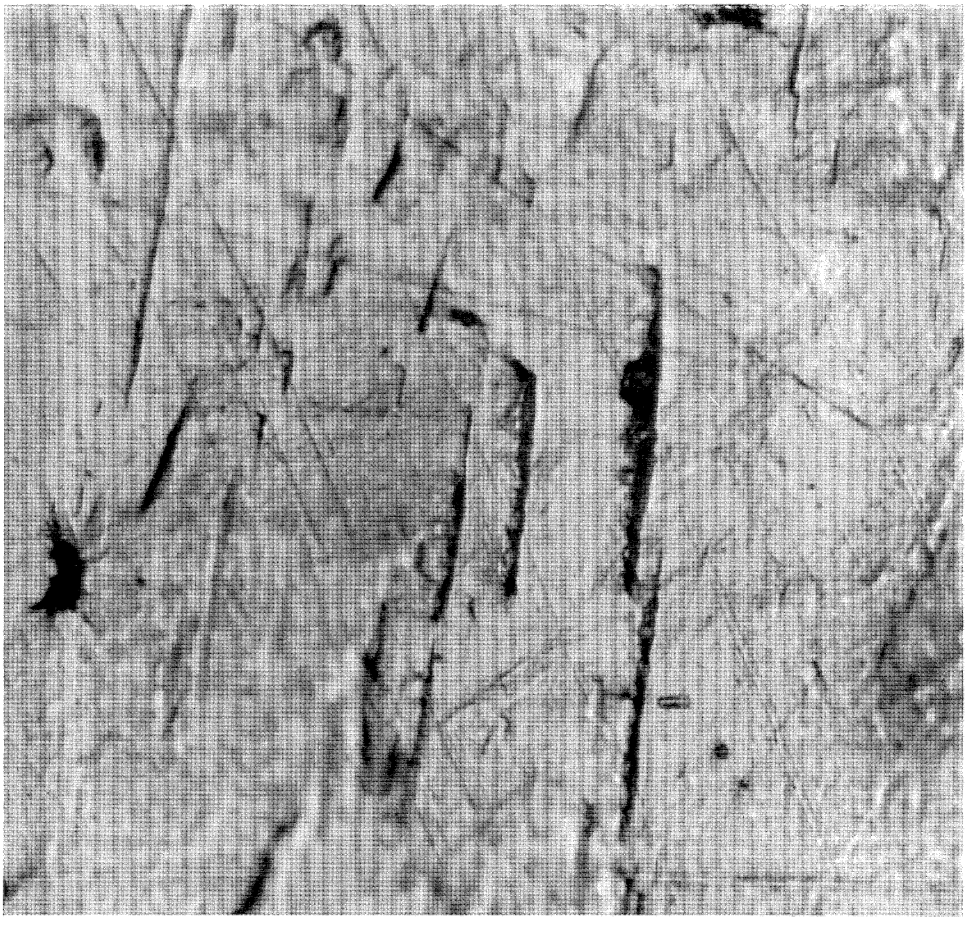

FIGURE 21. Shear deformation along twin boundaries in an iron single crystal. The centre of impact was to the right of the area photographed. $2{\cdot}8 \times 10^5$ impacts at 85 m/s. (Magn. $\times 470$.)

where P is the pressure and ρ the density of the liquid. This is the maximum pressure exerted during the impact. The force/unit length, F, along the specimen at this stage is:

$$F = \rho C V 2r\, V/C. \tag{8}$$

When the limit given by (5) is exceeded, outward flow becomes possible. The behaviour is now more complex and simple explanations are no longer satisfactory. For the final stages of impact when the impact plate is approximately half way through the cylinder, we can expect full incompressible flow to be established. The maximum pressure will then occur along the central stagnation line and be given by

$$P = \tfrac{1}{2}\rho V^2. \tag{9}$$

In addition to the normal forces acting on the surface there are shear forces associated with the high speed flow across the surface. In the velocity range covered in the experiments described here, the outward flow velocities are in the region of 100 to 400 m/s. For water flowing at these velocities over a smooth surface the shear forces are too small to cause damage. If the surface, however, is stepped or broken in any way, very large shear forces are produced by the impingement of the flow against the projections in the surface. For impact velocities which are as low as 90 m/s the shear forces acting on a roughened surface are normally large enough to cause local shear fractures, even in high strength materials.

To summarize the force distribution on impact: initially a small central area of first contact is compressed under a uniform pressure. The magnitude of the pressure is given by the water-hammer equation (3), and the width of the area affected by equation (6). The initial area of contact grows as the impact continues; there is very little reduction in pressure on the surface until appreciable outward flow begins at some critical value of the liquid/solid interface angle. At this stage there is a rapid fall in pressure along the periphery of contact. As the outward flow continues the water-hammer compression at the centre of impact is relieved until eventually the maximum pressure acting on the surface is the central stagnation pressure for incompressible flow (equation (9)). Large shear forces can occur as a result of the outward flow impinging against projections in the impact surface.

Measurement of the distribution and magnitude of the impact forces

Information on the distribution of forces acting on a plane rigid surface striking the side of a liquid cylinder can be obtained from an examination of the impact mark left on the solid. In order to produce a simple well defined mark in one impact it is necessary to use a relatively high impact velocity and a dense liquid jet. This was achieved by firing a polished polymethylmethacrylate specimen at a velocity of 150 m/s through a 1 mm diameter jet of mercury. Examples of the marks produced are shown in figures 4 and 5, plate 16. Figure 4 is a photograph taken in reflected light and figure 5 in transmitted light.

In all erosion marks of this kind there existed a central region of the impact area which was quite flat and in no way deformed. This area can be seen in figure 4 to lie between two faint horizontal lines running across the centre of the damaged zone. Outside this area the surface is broken by faint cracks parallel to the lines, and farther away still by two deep fractures one either side of the centre. The surface outside the deep fractures is increasingly

broken by a pitting action. The shape of the pits indicates that this is due to an outward acting shear force arising from the liquid flow across the surface. A similar experiment with soft aluminium specimens produced mainly smooth depressions. The depressions were compared with those formed by pressing a 1 mm diameter steel cylinder into the surface. They were found to be similar in size and shape, although the jet indentations were on average shallower and had their sides and rim distorted by the outward liquid flow.

The damage marks in the brittle and ductile materials suggest a Hertzian pressure distribution under the jet of the type associated with a hard cylindrical indenter. The simplest model of the impact which would account for these observations is one in which the jet deforms elastically (that is as a hard cylindrical indenter) up to the stage where considerable flow sets in. This is essentially the same model as that proposed in the preceding section from considering the deformation of the liquid.

The distribution of shear pits in the polymethylmethacrylate specimens indicates that liquid flow across the surface does not occur to any appreciable degree in the area between the main fractures (figures 4 and 5), but that it increases rapidly outside these lines to reach a maximum at some little distance from them. The line along which appreciable sideways flow begins can be obtained from the distribution of shear pits in the surface. Table 1 sets out measurements of this line for a range of velocities and jet diameters. The

TABLE 1. VALUES OF THE INTERFACE ANGLE β FOR WHICH FLOW FIRST DEFORMS THE SURFACE

jet diameter (mm)	velocity of impact (m/s)	angle
mercury jet 1	183	17° 15′
	169	16° 45′
	154	17° 0′
	152	16′ 45′
water jet 2·54	80	17° 15′
	65	17° 0′
water jet 1·35	80	17° 15′
	65	16° 15′
	55	17° 45′
	30	16° 0′
water jet 0·42	70	17° 0′
	55	16° 45′
	49	18° 0′
	38	17° 0′

results are expressed in terms of an angle β which is the angle subtended at the centre of the jet between the line of first contact and the line along which flow begins. The values of the angle β, somewhat surprisingly, show little change over a wide range of impact conditions. It may be noted that the values of β given in table 1 are considerably greater than those predicted by equation (5). For a 1·3 mm diameter water jet and an impact velocity of 60 m/s, β has a value of 2° 20′ by equation (5), whereas the experimental value is in the region of 17°. The lack of agreement may be due to the oversimplified analysis. Possibly because of the effects of viscosity, the liquid fails to flow at very small values of β.

Direct measurements were made of the impact load itself, using a barium titanate pressure transducer in place of the specimen in the wheel and jet apparatus. The output of the crystal was taken from the rotating disk with carbon brushes and displayed on an oscilloscope screen. The transducer was calibrated by using the impact of falling metal rods after the manner of Crook (1952). A typical load-time trace is shown in figure 6. The impact velocity in this case was 61 m/s and the jet diameter 1·3 mm.

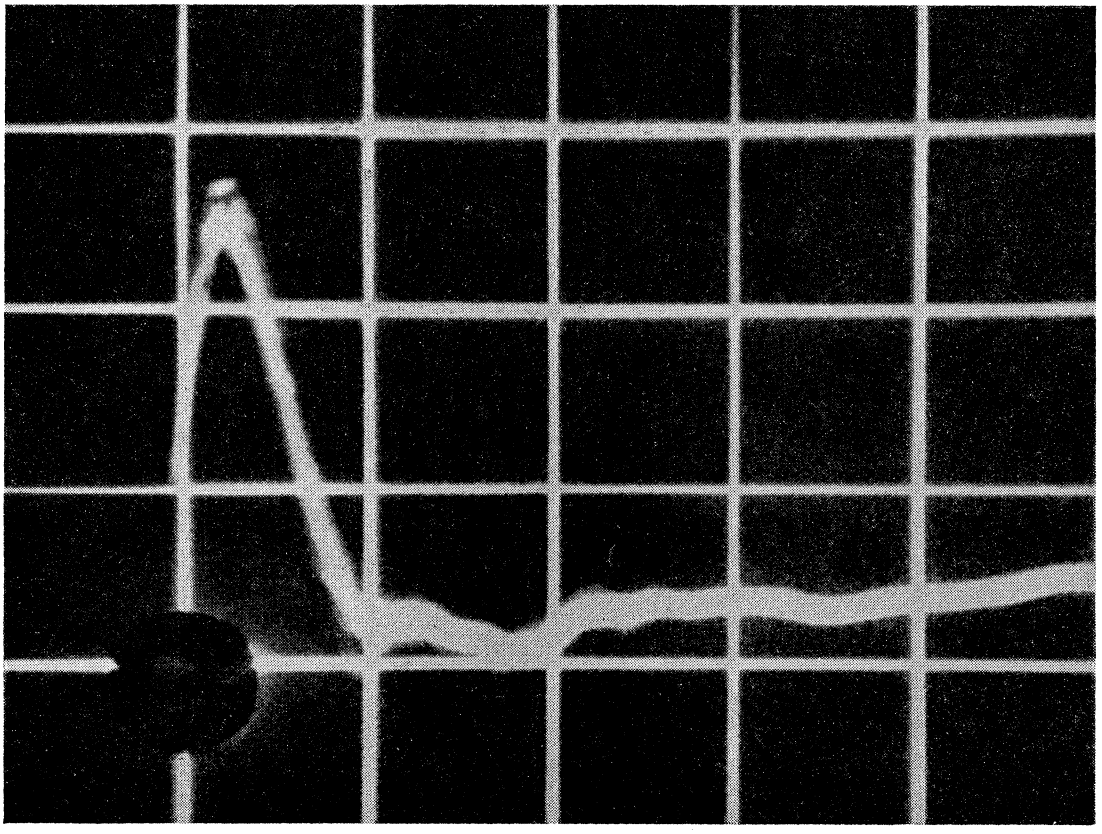

FIGURE 6. A load–time trace for a liquid impact at a velocity of 61 m/s and a water jet diameter of 1·3 mm. One vertical division = 14 Kg. One horizontal division = 5 μs.

The maximum impact load measured as a function of impact velocity for three different diameters water jets is shown in figure 7. The experimental measurements are given together with the estimated error. The dashed lines represent the calculated variation of maximum load with velocity on the assumption that the maximum occurs just at the instant flow begins ($\beta = 17°$) and that the pressure up to this point is the water-hammer pressure. The agreement is reasonably good.

EROSION DAMAGE IN NON-METALS

The erosion of polymethylmethacrylate

A study was made by means of the wheel and jet apparatus of the erosion process in selected polymers and ceramics. Polymethylmethacrylate was found to be a convenient material for part of this study owing to the ease with which suitably polished specimens

could be prepared, and eroded. For the most part a 1·3 mm diameter water jet was used as the eroding liquid. Measurements of the erosion damage were made with the light meter and an optical microscope.

The first evidence of erosion was usually the appearance of two fine bands of fracture on either side of the central line of impact and lying parallel to the long axis of the jet. With successive impacts these fractures increased in number and many of them chipped away along their outer edges to form pits in the surface. An illustration of a specimen in this

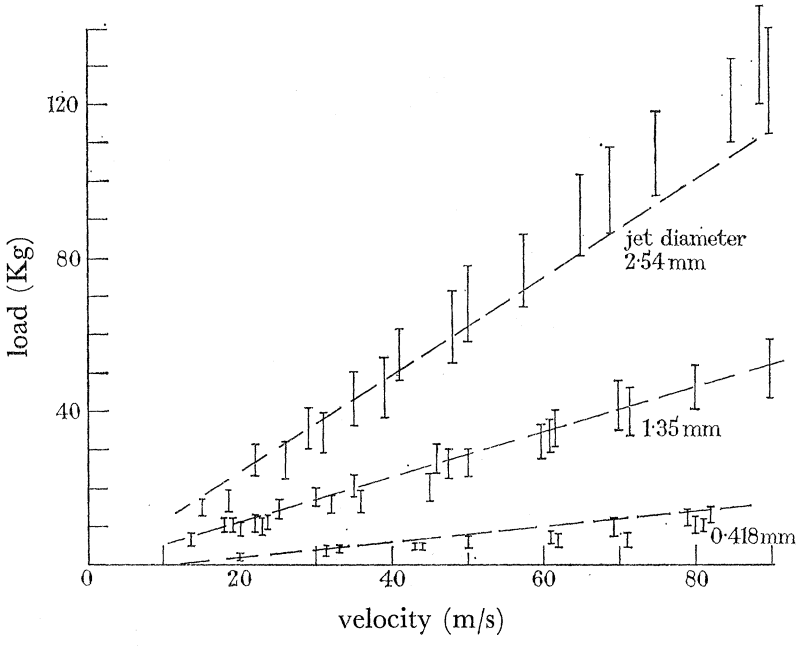

FIGURE 7. Variation of the impact force with velocity and jet diameter. I, Experimentally determined value; - - -, calculated variation of load with velocity.

condition after 3500 impacts at 68 m/s is given in figure 8, plate 17. There is an obvious similarity in pattern here to the photographs in figures 4 and 5. In the multiple impact example the pattern is less well defined, presumably because the centre line of impact shifts slightly from impact to impact. The fractures produced in this way form small steps in the surface along their length. The outward flowing liquid strikes against the steps and erodes away the edges to leave a pit. This mechanism has been discussed in an earlier paper (Bowden & Brunton 1961). The pits from the individual fractures eventually join up to form deep channels on either side of a relatively undamaged central area (figure 9, plate 17). With further impacts the central region is eventually undermined and eroded away.

Angle of entry

The fracture pattern was found to be very dependent upon the angle of entry of the specimen into the jet. If the specimen was tilted slightly so that either the top edge or bottom edge entered the jet first, then the two parallel bands of fracture produced in normal impact gave way to a curved system of fractures lying concave to the point of initial entry. The concave system is shown in figure 10, plate 18. In this case the line of impact runs centrally from the bottom to the top of the photograph with the lower edge of

the specimen (bottom of the photograph) having struck the jet first. The tilt angle in this example was 9°. The concave pattern arises from the tensile stresses across the concave boundary line of the instantaneous area of contact between the jet and the specimen.

The change in erosion with time

The erosion damage of polymethylmethacrylate (measured with the lightmeter) as a function of the number of impacts is shown in figure 11. A feature common to curves of this kind is the initial delay period during which there is no apparent change in the surface structure. The erosion rate thereafter stays constant. The measurements shown here refer to the very early stages of erosion. Appreciable weight loss does not occur until a reflexion coefficient of about 75 % is reached.

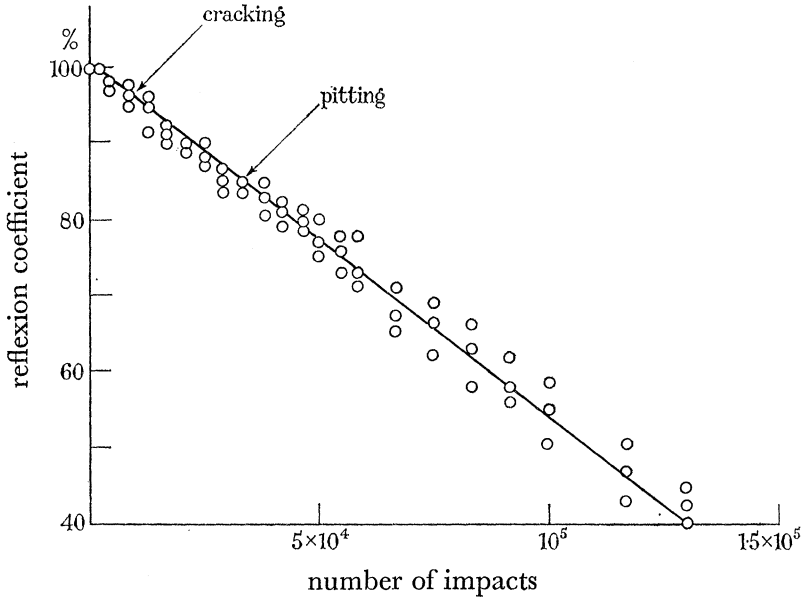

FIGURE 11. Development of erosion damage with number of impacts in polymethylmethacrylate. Water jet diameter, 1·35 mm.

Impact velocity

The effect of impact velocity on the amount of erosion at two different exposure intervals is shown in figure 12. For this particular material the erosion rate varied as the velocity of impact raised to the power 4·5. This may be compared with a figure of 3·4 obtained from gravimetric measurements by Fyall *et al.* (1956–57). A threshold velocity of 24 m/s was found below which damage was not produced even after very long duration runs.

Surface roughness

Surfaces of polymethylmethacrylate were polished with finishes corresponding to abrasive particle sizes of 30, 14 and 1 μm and then eroded at 60 m/s with 1·3 mm diameter water jet. The erosion/time curves were identical for the 30 and 14 μm particles, the 1 μm finish, however, required 3·3 times as many impacts to produce pitting under the same

conditions. In examining the effect of surface finish, it was found that coarse polishing marks often gave rise to erosion fractures along their length and occasionally to shear pitting. A coarse finish could in this way alter the normal erosion pattern.

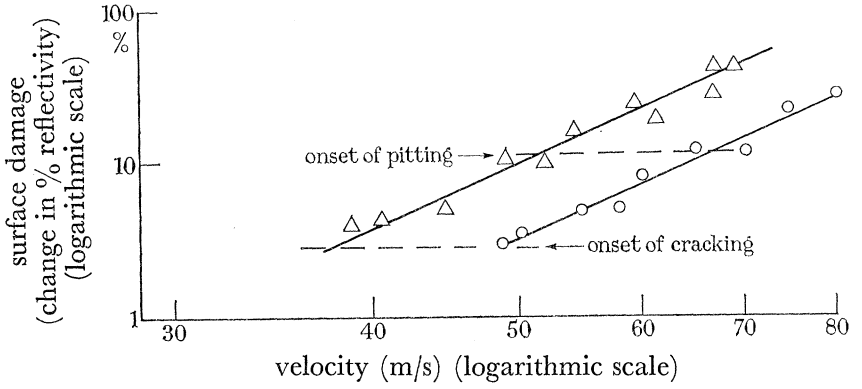

FIGURE 12. The effect of the impact velocity on the amount of erosion in polymethylmethacrylate at two different intervals of exposure. ○, Deformation after 10000 impacts; △, deformation after 50000 impacts. Water jet diameter, 1·35 mm.

The size of the jet and the area of erosion

The effect of altering the size of the jet on the time taken to reach a certain stage in the erosion process was investigated. Figure 13 shows the variation in the number of impacts which are necessary to just produce detectable fracture in the surface for different diameter water jets. The impact velocity was 56 m/s in each case. As the jets become smaller it can be seen that their damaging effect becomes less. This result is thought to be due to a reduction in the duration of the initial impact load with a decrease in the jet diameter.

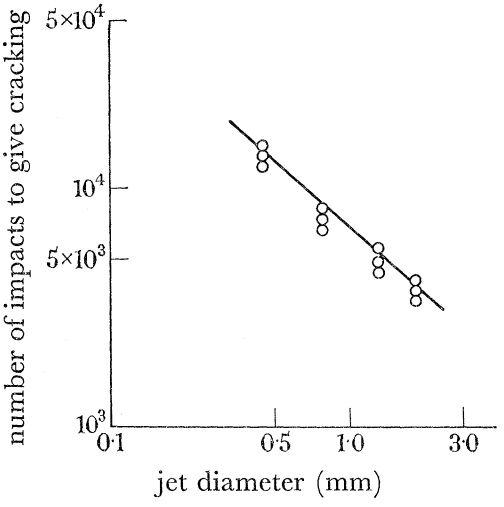

FIGURE 13. The effect of altering the jet diameter on erosion.

The duration of the impact load can also be reduced by making the width of the impact area appreciably smaller than the diameter of the jet. It was found that a long thin specimen with a width equal to one-tenth of the jet diameter was completely unaffected after the order of 10^5 impacts. Whereas under the same conditions a specimen with a large

impact area became deeply grooved. The resistance to damage of thin specimens was the same whether they were eroded with their lengths at right angles to or parallel with the long axis of the jet.

Ceramics and inorganic single crystals

Similar behaviour to that described above for polymethylmethacrylate has been observed in other hard polymers and ceramics. While the pattern of failure was much the same throughout, the number of impacts required to produce equivalent amounts of erosion damage varied considerably from material to material. In soda-lime glass, for example, 10^5 impacts at 80 m/s were necessary before the first fine pits and cracks appeared (cf. 10^3 impacts with polymethylmethacrylate). With sintered alumina 6×10^5 impacts at 90 m/s were necessary before the first signs of damage appeared. As with most of the sintered materials examined, erosion occurred by the removal of individual sintered particles. Although it took a relatively long time to form these initial pits, erosion occurred very rapidly after the formation of the first few pits.

It is of interest to note that diamond and silicon carbide crystals were undamaged after 5×10^6 impacts at 95 m/s. These were the only materials which remained entirely unaffected at this impact velocity.

Experiments were carried out on the erosion of some relatively soft inorganic single crystals, including calcite, fluorite and apatite. A critical impact velocity for each of these materials was found below which no evidence of deformation of any kind could be detected after a long exposure (10^6 to 10^7 impacts). Above this critical velocity the specimen failed by tensile cracking in very short periods of time. The critical velocity for calcite was 36 m/s and for apatite and fluorite 40 to 43 m/s. The existence of a critical impact velocity for failure is an interesting property of these materials and distinguishes them in a very definite way from hard polymers and metals.

Discussion of the erosion of brittle solids

If during the initial stages of impact we regard the jet as a hard indenter, then the pressure distribution will be such that the maximum compressive stress acts along the centre line of impact. The compressive stress falls to zero and changes to a tensile stress along the line where the outward flow begins. The maximum tensile stress will be at the surface and will act at right angles to this line. Thus in a brittle solid, the central region will be elastically compressed, while the first fractures will appear along the boundaries of this region, where the outward flow begins.

For a cylindrical indenter pressed against a hard surface, the maximum tensile stress along the boundary of the area of contact is approximately one-tenth of the maximum compressive stress at the centre of the contact area. For a liquid jet, assuming it behaves initially in a compressible manner, the maximum tensile stress will be approximately one-tenth of the water-hammer pressure. The minimum impact velocity $V_{\text{min.}}$ to cause fracture in one impact will then be, by equation (3),

$$V_{\text{min.}} = 10T\left[\frac{\rho_s C_s + \rho C}{\rho_s C_s \rho C}\right], \tag{10}$$

where T is the breaking strength of the solid. Single impact experiments with mercury and water jets and polymethylmethacrylate specimens, showed that below the minimum velocity for water fractures were not observed, and above this critical velocity (for mercury about 70 m/s) fractures were found. No definite bracket for a critical velocity for fracture was established.

Under repeated impact conditions fractures were produced at impact velocities well below the estimated minimum. In polymethylmethacrylate erosion fractures occurred at an impact velocity of 24 m/s, yet in the single impact experiments no detectable damage was produced at 10 times this velocity. The gradual appearance of fractures at low velocities could generally be traced back to initiation at surface flaws. Erosion at low velocities is not unlike a fatigue process. The average stress may be too low to cause general failure, but in regions of stress concentration some deformation is produced by each impact. The amount of deformation is cumulative and after several thousand impacts—the incubation period—the cracks can just be detected. When the surface is sufficiently roughened by fractures of this kind, erosion of the surface by the outward flowing liquid begins.

In the experiments with the inorganic crystals calcite, apatite and fluorite, a critical velocity was found below which the specimens showed no signs of failure after 10^6 to 10^7 impacts, and above which they failed rapidly. In these crystals it is thought that surface flaws are less important and that below the critical velocity the breaking stress of the crystals is not reached.

The erosion of metals

Copper and its alloys

Specimens of copper were prepared in the form of small bars machined from a copper rod containing less than 0·001 % impurity. The specimens were annealed at 850 °C and then furnace cooled. The impact surface was polished prior to erosion.

For impact velocities in the range 30 to 90 m/s and with a 1·3 mm diameter water jet, the first signs of damage were detected after several thousand impacts. The area of impact was found to be covered by randomly distributed depressions. An example is shown in figure 14, plate 18. The depressions varied somewhat in shape but it was usual to find that the bottom of the depression formed a linear fault in the surface. Maximum dimensions of these depressions lay in the range 5 to 15 μm. The position of the depressions was not related in any obvious way to grain or phase boundaries or to grain orientation and their size and distribution was not affected by different surface preparations. It was found that for the same exposure there were far fewer depressions in single crystals than in the corresponding polycrystalline specimens.

With further exposure in the erosion apparatus it was possible to distinguish grain and phase boundaries. The overall effect was very similar to that produced by a chemical etching of the surface. The appearance of the grain boundaries is thought to be due to the differing amounts of plastic deformation within each grain and not to a chemical attack of the surface.

The initial stages in the erosion process are illustrated in figure 15, plate 19. The depressions are just visible after 5160 impacts, while after 51 600 impacts, the grain boundaries are clearly visible.

The third stage of erosion follows on rapidly from the first two. The rate of deformation and removal of material from the surface increased under the action of liquid flow along the surface. The shear damage caused by this was confined entirely to regions of surface unevenness produced in the first two stages of erosion. Thus grain and phase boundaries, slip and twin traces, and depressions in the surface provided sites for rapid erosion. In copper the final stage of erosion involved a ductile tearing of the metal.

The rate of erosion is limited by the number of suitable sites where deformation can occur. In single crystals of copper, for example, the absence of grain boundaries led to a decrease in the total number of erosion pits present in the surface compared with the number observed in polycrystalline copper. In 60/40 brass the $\alpha\beta$ phase boundaries provided suitable sites for pitting, so that the overall density of pitting was greater than in copper.

In the 60/40 alloy, a network of cracks formed in the β phase and ran into the body of the specimens from the roots of the surface pits. Well defined slip lines were also visible during the very early stages of erosion. Neither of these effects was found in copper.

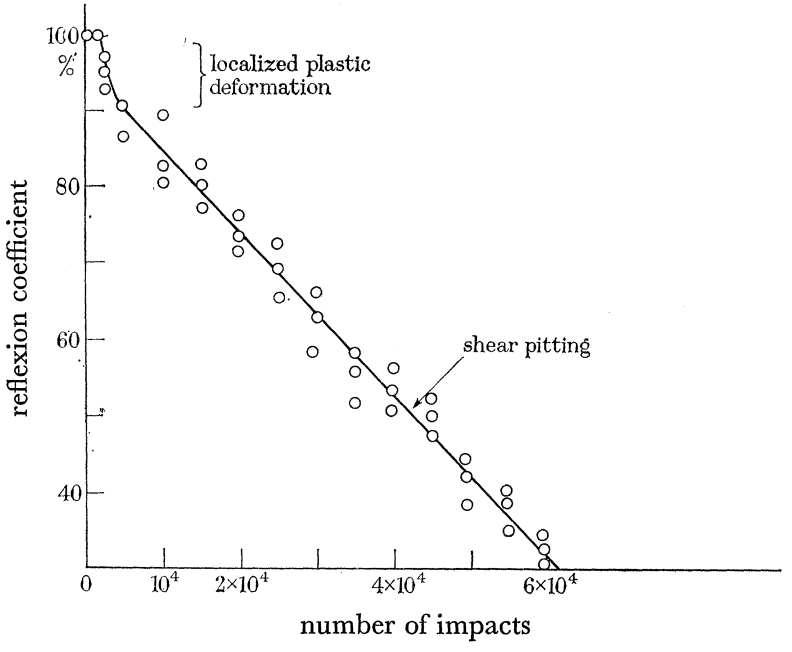

FIGURE 16. Development of erosion damage with number of impacts in copper. Water jet diameter, 1·35 mm.

The effect of the number of impacts and the impact velocity on erosion

The results obtained for the surface deformation of copper (measured with the light-meter) as a function of the number of impacts and the velocity of impact are shown in figures 16 and 17. The general behaviour, in spite of a considerable difference in the mechanism of failure, is similar to that found for the hard polymers. It can be seen in figure 16 that as with polymethylmethacrylate, there is a quiescent period during which no detectable change occurs in the surface—this is followed by the fairly sudden appearance

of depressions and grain boundaries and finally by large erosion pits. A study of the velocity relation (figure 17) showed that the deformation increases as the velocity raised to the power 2·7.

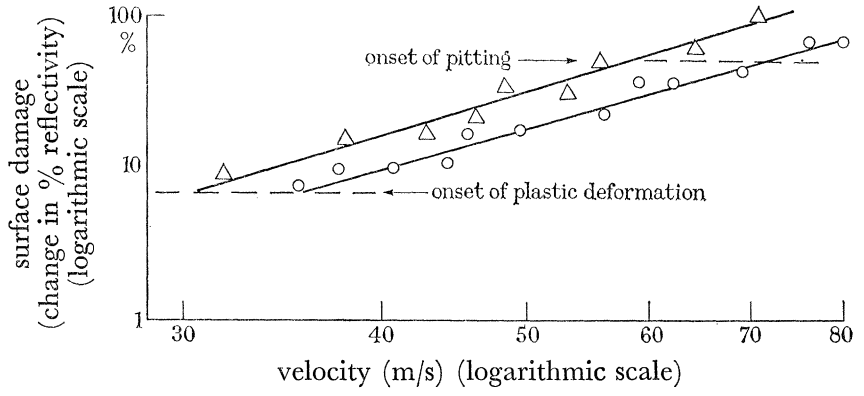

FIGURE 17. The effect of impact velocity on the erosion of copper. ○, Deformation after 20000 impacts; △, deformation after 50000 impacts. Water jet diameter, 1·35 mm.

The effect of hardness on erosion

In this experiment specimens of annealed copper were cold rolled to give reductions in area of up to 50%. This gave a corresponding range in Vickers hardness of 80 to 168 Kg/mm^2. The number of impacts necessary to produce a certain degree of surface deformation (in this case a surface reflectivity equal to 50% of that of the polished surface corresponding approximately to the stage where pits begin to form) was determined for specimens of different hardnesses. The slope of the curve was found to be very nearly unity.

In determining the effect of hardness on erosion, work hardening due to the erosion itself must be considered. In annealed copper, for example, it was found from microhardness measurements that in the eroded region the mean hardness was approximately twice that in the surrounding area.

The erosion of aluminium

The general pattern of failure in aluminium was found to be very similar to that in copper. With aluminium an experiment was carried out to examine the effect of grain size on erosion behaviour. The results are shown in figure 18. The specimens were of similar purity. In the polycrystalline material the variation in grain size was produced by cold rolling and annealing to bring about recrystallization. The mean microhardness values for small grained, large grained and single crystal specimens were 42, 30 and 27 Kg/mm^2 respectively. It was found that in spite of a lower hardness the single crystals had a greater resistance to erosion than the large grained specimens. This again emphasizes the importance of grain and phase boundaries in causing pitting.

The erosion of iron and its alloys

For the wide range of steels examined it was found that the erosion process was identical with that outlined in the previous examples. The main difference showed itself as a general

increase in the resistance to deformation. As in the previous examples it was found that depressions were formed initially and that these were further deformed by the outward flow. This secondary deformation was more intense at some distance from the centre line of impact. The two bands of heavier damage in a low carbon steel can be seen in figure 19, plate 20. At a later stage it was possible to section through some of the larger pits and examine the structure beneath the surface. A transgranular system of fractures was found to spread out from the roots of the pits. An example of this is shown in figure 20, plate 20.

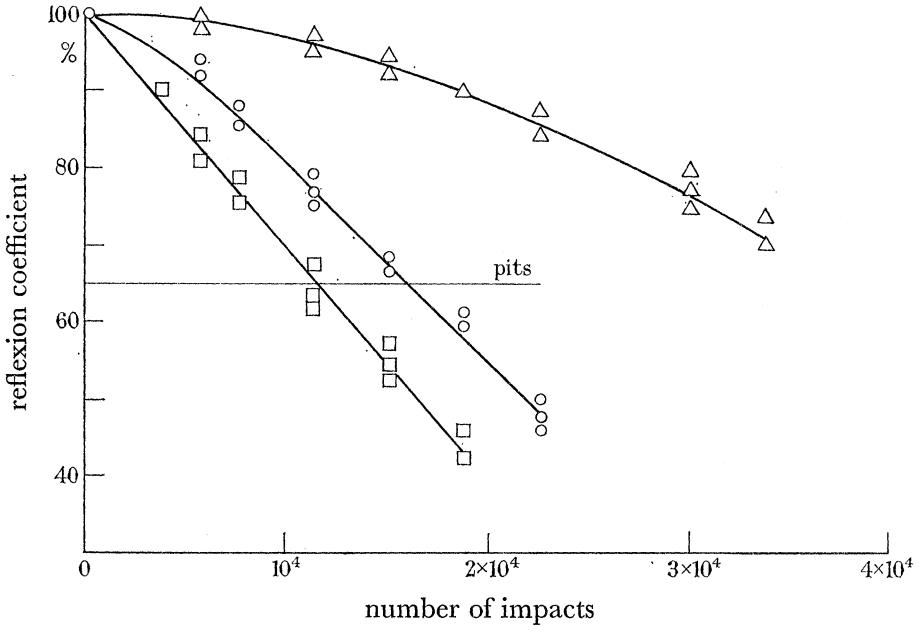

FIGURE 18. The effect of grain size on the erosion of pure aluminium. △, Small grain size (0·0045 mm); ○, single crystal; □, large grain size (0·045 mm).

The fractures lengthened with further exposure to impact and gradually undermined the surface. Brittle fracture of metal near the surface is considered to be the principal mechanism of failure in this final stage of erosion.

The same pattern of failure was found in an 18/8 austenitic stainless steel. The time taken to produce pits in this steel was greater than in the low carbon steel by a factor of 3—presumably due to the greater hardness 400 Kg/mm^2 compared with 200 Kg/mm^2 in the carbon steel.

In a very hard alloy cast iron, hardness number 730 Kg/mm^2, and composition 3·6% C, 5% Co, 4·8% V, 1·32% W, 1·01% Mo, 0·6% Mn, no evidence of depressions or plastic deformation was found after 10^6 impacts at 98 m/s. A dulling of the surface was found to be due to a mechanical etching effect caused by the very slight tilting of the individual grains. Occasionally a pit was formed by the removal of a carbide particle. This very slight damage was considered to be due entirely to the outward liquid flow.

The behaviour of a single crystal of iron was examined in the wheel and jet apparatus. The iron crystal was grown by the strain anneal method and contained 0·003% C with traces of manganese, silicon, sulphur and phosphorus. The specimen was eroded at 85 m/s. The first signs of deformation were again small depressions in the surface. The density of

depressions was reduced by a factor of 8 to 10 compared with a corresponding polycrystalline specimen. After the order of 10^5 impacts twins appeared in the surface; these were further deformed by the flow across the surface. Twins sheared in this way are shown in figure 21, plate 21. The pits produced along the twin steps were found, when sectioned, to have fractures running out from their tips. Perhaps the most remarkable feature about the deformation of the iron crystal was its excellent erosion resistance in spite of the low hardness value of 85 Kg/mm^2. Irrespective of the method of measurement the deformation of the crystal at any stage during the erosion process was no more than that found with austenitic steel (hardness 400 Kg/mm^2) at the higher impact velocity. In the absence of twin steps in the surface it is very likely that an even greater erosion resistance would have been observed.

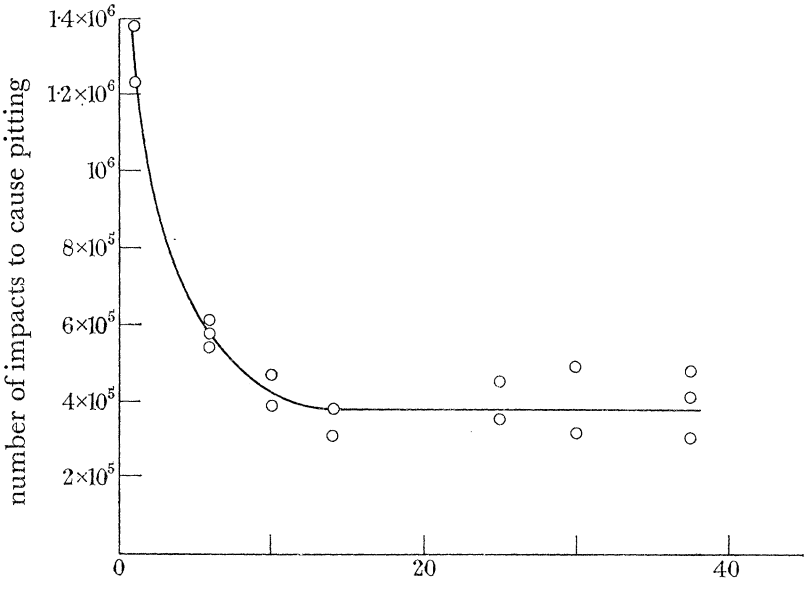

FIGURE 22. The effect of surface finish on the number of impacts required to produce erosion pits in 18/8 austenitic stainless steel.

The effect of surface finish on the erosion of 18/8 *stainless steel*

Specimens of the austenitic steel were prepared with scratch finishes varying from 37 μm down to 1 μm. The number of impacts necessary to produce pits and remove metal from the surface was measured for the different finishes. The results shown in figure 22 refer to an impact velocity of 90 m/s and a 1·3 mm diameter water jet. It can be seen that the finish has very little effect above 12 μm. Finer finishes have a considerable effect on the rate of damage; a 1 μm finish requires an exposure nearly 4 times greater than a 12 μm finish to bring about equivalent damage.

The erosion of stellite

Stellite is an alloy with considerable erosion resistance. It is used a great deal by the turbine industry to protect blade edges. In the present study the particular cast alloy which was used had the composition 66% cobalt, 26% chromium, 5% tungsten and 1% carbon. Polished specimens were eroded at 94 m/s by means of a 1·3 mm diameter water

jet. The dendritic structure 'etched' up after about 10^5 impacts, but there was no evidence of depressions in the surface or of pitting even after 10^6 impacts. This behaviour may be compared with that of 18/8 stainless steel of comparable hardness under the same conditions. The stainless steel showed depressions after 10^3 impacts. Later the structure 'etched', and at 10^5 impacts the surface was pitted and metal had been eroded away.

Discussion of the erosion of metals

Erosion in metals begins with a roughening of the surface. This has been shown to be due to the appearance of small surface depressions and to the tilting of the grains. The larger projections in the roughened surface are later sheared by the flow to give surface pits. The pits grow and erosion continues either by a ductile tearing action or by the propagation of brittle fractures from the bottom of the pits.

The appearance of surface depressions is thought to reflect non-uniformity in the strength of the surface rather than non-uniformity in the applied load. The latter would occur, for example, if the metal or jet surface was rough, or if cavitation was present in the flow. Neither of these effects have been detected. Furthermore in relatively isotropic solids such as hard polymers and glasses, there has been no evidence of local failure or fracture which would correspond to the plastic depressions in metals. Non-uniformity in the yield strength and hardness of polycrystalline metal surfaces, on the other hand, is to be expected. Grain orientation and the existence of defect structures within the grains will lead to considerable inhomogeneity in the flow stress on a microscale. Some slight variation in flow stress can be detected from microhardness indentations at light loads. The differences in hardness are generally too small, however, to account for the marked differences in erosion behaviour. Possibly with smaller indentations a larger hardness variation would be observed.

The existence of soft spots would explain why a high strength metal—for example, a cold rolled stainless steel with a yield strength in the region of 11 000 Kg/cm^2 erodes at a velocity of 90 m/s and at a maximum water-hammer pressure of 1300 Kg/cm^2. Or again why a cold rolled copper specimen with an average yield strength of 400 Kg/cm^2 is eroded at 24 m/s at a maximum impact pressure of 340 Kg/cm^2. In these examples each impact will produce some local yielding at soft spots. Some of the depressions which are produced either because of their size or shape will cause stress concentration and so experience a greater pressure than average. These depressions will grow at a greater rate. The more they deform, the greater will be the stress causing deformation. Plastic deformation of the surface within the grains eventually shows up the grain boundaries and gives the surface an etched appearance.

The surface roughened by depressions and grain boundaries is further eroded by the shearing action of the outward flow. This type of deformation is most intense on either side of the central area (figure 19) where the flow velocity is greatest. The larger depressions and most prominent grain boundaries erode to form pits in the surface. It was found that in the single crystals of iron and aluminium the absence of grain boundaries noticeably reduced the rate of shear damage.

The final stage of erosion in metals is the growth of pits throughout the specimen—a stage which is accompanied by appreciable weight loss. The presence of a pit on the

surface will give rise to stress concentration at the root of the pit. In metals which are prone to brittle fracture the stress concentration leads to the formation of a network of cracks which fan out from the pit (figure 20). The cracks propagate slowly—usually along crystallographic directions within the grains. With more ductile metals erosion proceeds by shear fractures in the metal around the pits.

The erosion of metals depends entirely on the initial formation of small regions of plastic deformation. If a metal surface can be kept smooth by preventing roughening due to depressions and grain boundaries, then the erosive action due to outward flow cannot take place. Roughening is minimized in single crystals where relatively few depressions form. For example, in the single crystal of iron, erosion occurs mainly along deformation structures such as twins and slip lines. It seems, however, that in plastically deforming materials a few local areas can be deformed at stress levels considerably below the average flow stress. As soon as this happens, the change in the shape of the surface leads to stress concentration at projections and depressions, the impact stresses increase, and ductile or brittle fracture brings about erosion.

The influence of the properties of the liquid on erosion

Experiments with carbon tetrachloride as the eroding medium showed that while there was no appreciable change in the form of damage, the erosion rate was approximately twice the rate with mains water. The effect is thought to be due to the higher density of carbon tetrachloride (1·69 g/cm^3).

It was found that chemically active solutions generally lead to an increase in erosion damage. For example, an aqueous salt solution (35 parts/1000 NaCl) eroded steel 1·8 times faster than mains water. On the other hand, the rate of erosion of copper was the same in brine as in water.

Altering the temperature of the liquid affected erosion rates in both metals and non-metals. In all cases the higher temperatures increased the surface shear damage produced by the outward flow. The increase is probably due to the reduction in viscosity of the liquid at the higher temperatures. It should be emphasized that changing the temperature of the water affected mainly the shear damage, the number of impacts to produce the first signs of deformation was unaffected.

Conclusion

From the experiments we have described, it is possible to classify the erosion behaviour of a material into one of two groups: materials which fail in a brittle manner in tension and those which deform plastically in shear.

In the case of brittle materials failure occurs by the slow propagation of fractures from surface flaws at stress levels which are often lower than the macroscopic breaking stress. The factors controlling the resistance to failure are the interatomic bond strength, the size and distribution of surface flaws, and the effect of the liquid environment on the surface energy of the solid and hence on the propagation of the fractures. It has been shown that a high bond strength and the absence of flaws leads to a good erosion resistance. This is the case with silicon carbide and diamond. Weaker crystals—such as apatite and fluorite, again show great resistance up to a critical impact velocity and then fail rapidly. Finally,

glasses and polymers, which as a class are particularly flaw sensitive, have no 'safe' impact velocity, but erode at extremely low velocities.

Metals and alloys as a group are also deformed at very low impact velocities. The first sign of erosion is the appearance of small surface depressions. These grow slowly until eventually metal is removed either by a ductile tearing or by brittle fracture of the roughened surface. The greater the yield strength (or hardness) the lower the deformation rate. The depressions are thought to be due to local yielding at 'soft spots' in the surface. The greatest resistance to erosion is found in those alloys which have a *uniformly* high yield strength as a result of a very fine grained microstructure. In the present work, the two alloys which showed the greatest erosion resistance were an alloy cast iron and a cobalt base stellite. The cast iron was very hard and brittle and was resistant to deformation by liquid impact for the same reasons as diamond. The stellite, on the other hand, was moderately hard (400 Kg/mm^2) but with some ductility. The fact that it did not show soft spots or erode is thought to be due to the fine distribution of carbides reinforcing the more ductile matrix. The deformation of stellites under hydrodynamic loading is still being investigated. The indications are that a high erosion resistance in a ductile alloy can be produced by the fine distribution of a hard second phase in a matrix which itself has a high rate of work hardening.

We wish to express our thanks to Professor F. P. Bowden, F.R.S., for his help and encouragement during the course of this work and to our colleagues in the Department of Surface Physics for many helpful discussions. We thank also the Central Electricity Generating Board for their support of the work.

References (Hancox & Brunton)

A.S.T.M. 1961 Symposium on erosion and cavitation. *A.S.T.M. Tech. publ.* no. 308.
Beal, J. L. & Wahl, N. E. 1951 *U.S. Air Force Tech. Rep.* no. 6190.
Bowden, F. P. & Brunton, J. H. 1961 *Proc. Roy. Soc.* A, **263**, 433.
Cook, S. S. 1928 *Proc. Roy. Soc.* A, **119**, 481.
Crook, A. W. 1952 *Proc. Roy. Soc.* A, **212**, 377.
De Haller, P. 1933 *Schweiz. Bauzg* **101**, 243, 260.
De Haller, P. 1940 *Schweiz. Arch.* **6**, 61.
Engel, O. G. 1955 *J. Res. Nat. Bur. Stand.* **54**, 51.
Engel, O. G. 1957 *W.A.D.C. Tech. Rep.* 53-192, PT 10.
Engel, O. G. 1958 *J. Res. Nat. Bur. Stand.* **61**, 47.
Engel, O. G. 1959 *J. Res. Nat. But. Stand.* **62**, 229.
Field, J. E. 1962 Ph.D. Thesis, Cambridge University.
Fyall, A. A., King, R. B. & Strain, R. N. C. 1956–57 *R. Aircr. Establ. Rep.* (*Chem.*), nos. 509, 510, 513.
Gardner, F. W. 1932 *The Engineer*, **153**, 146, 202.
Honegger, E. 1927 *Brown Boveri Rev.* **14**, no. 4, p. 95.
Jenkins, D. C. & Booker, J. D. 1958*a* *Tech. Notes, R. Aircr. Establ.* (*Mech. Eng.*), no 267.
Jenkins, D. C. & Booker, J. D. 1958*b* *Tech. Notes, R. Aircr. Establ.* (*Mech. Eng.*), no. 275.
Mochel, N. L. 1950 *Mechanical wear.* M.I.T. Cambridge, Mass.: Am. Soc. Metals.
Parsons, R. H. 1936 *The development of the Parsons steam turbine.* London: Constable.
Vater, M. 1937 *Z. Ver. dtsch. Ing.* **81**, 1305.
Von Schwarz, M. & Mantel, W. 1936 *Z. Ver. dtsch. Ing.* **80**, 863.

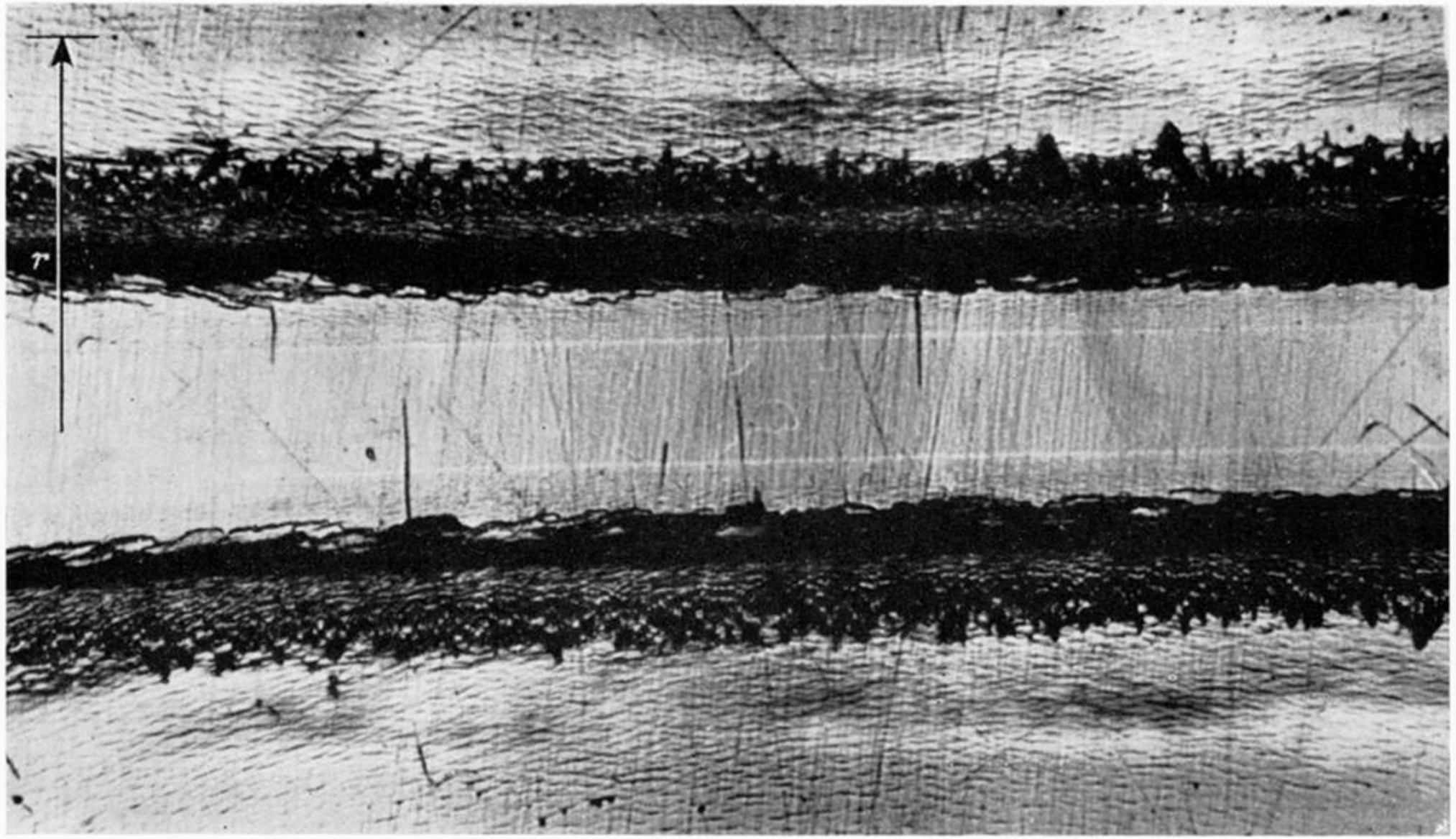

FIGURE 4. Deformation of a polymethylmethacrylate specimen which has been shot through a 1 mm diameter jet of mercury at 150 m/s. The radius of the jet is shown by the arrow. The photograph was taken with reflected light.

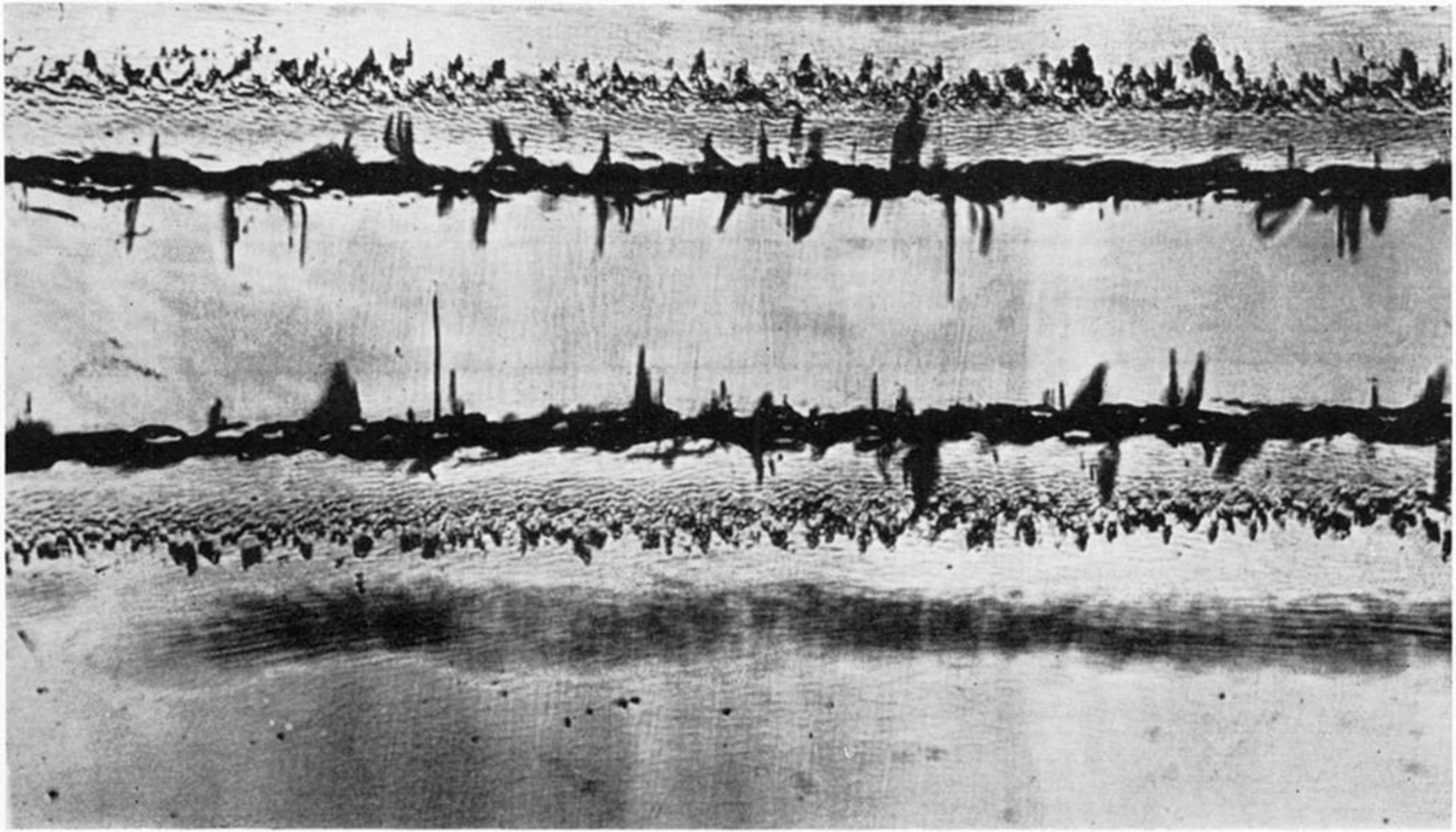

FIGURE 5. The same area as that shown in figure 4 but now photographed in transmitted light.

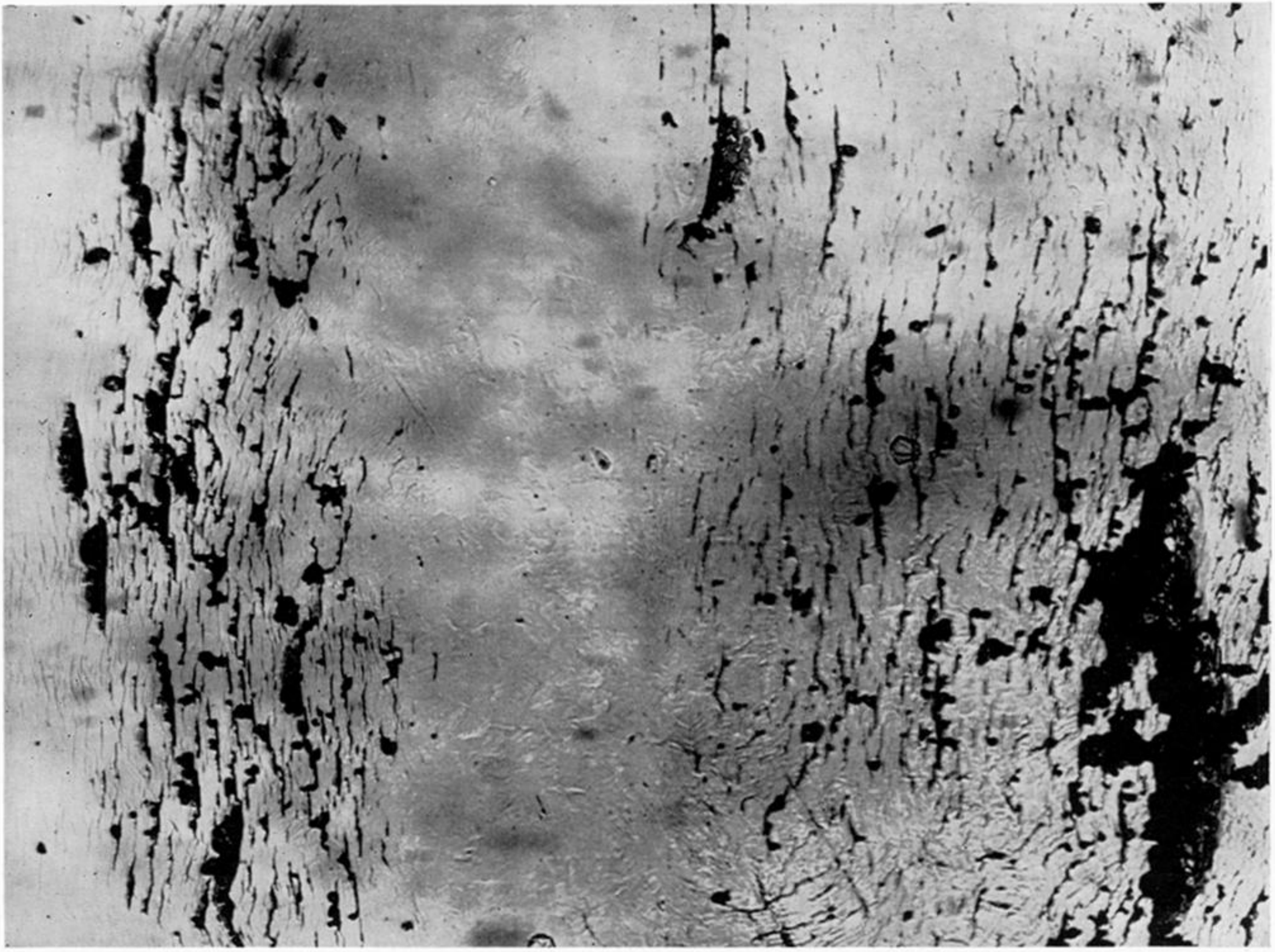

FIGURE 8. Fractures in a polymethylmethacrylate specimen after 3500 impacts at 68 m/s. The bands of fracture lie parallel to the jet axis.

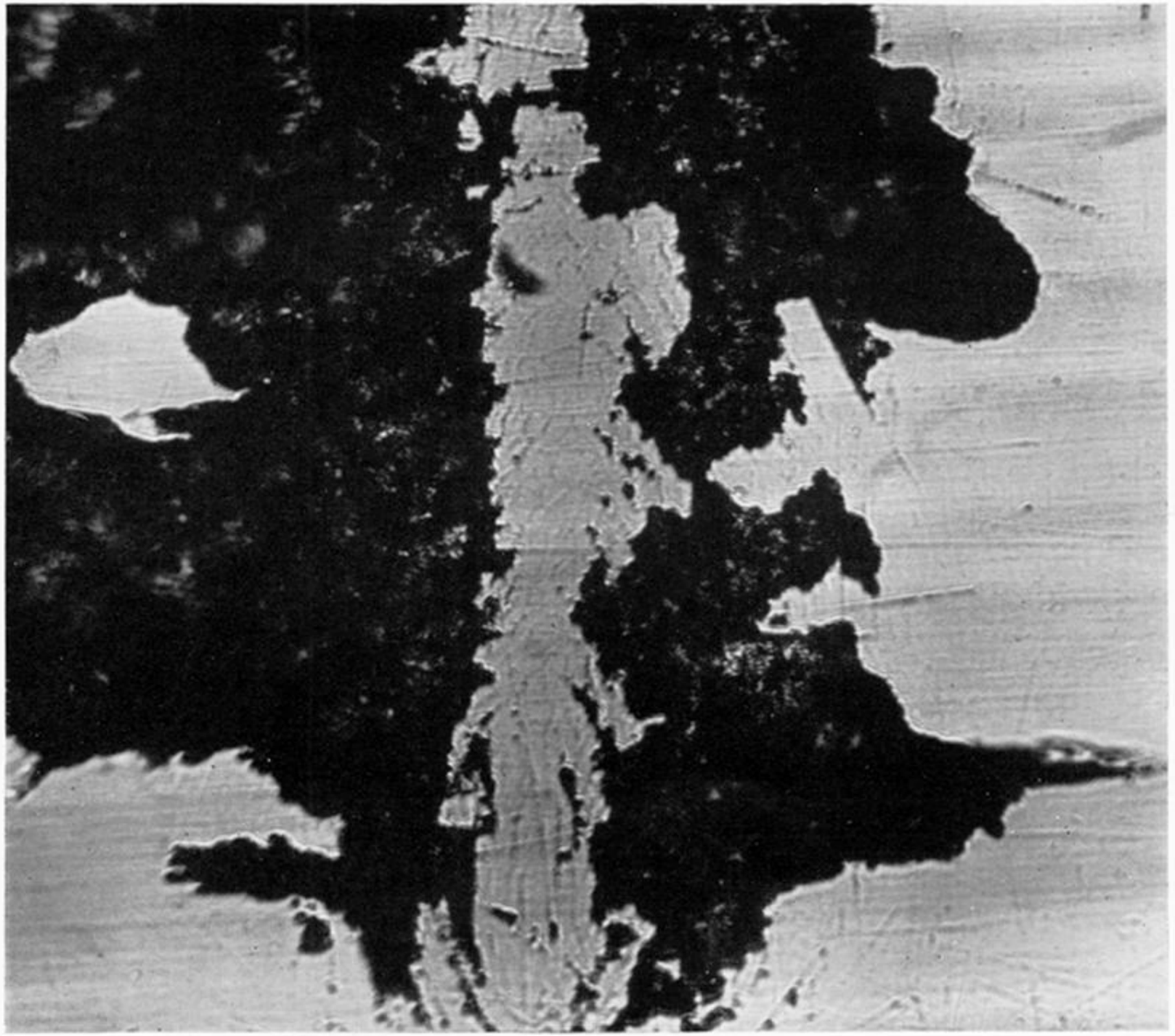

FIGURE 9. The surface of a heavily eroded polymethylmethacrylate specimen which has received 47 000 impacts at a velocity of 67 m/s. The central region is only lightly fractured at this stage.

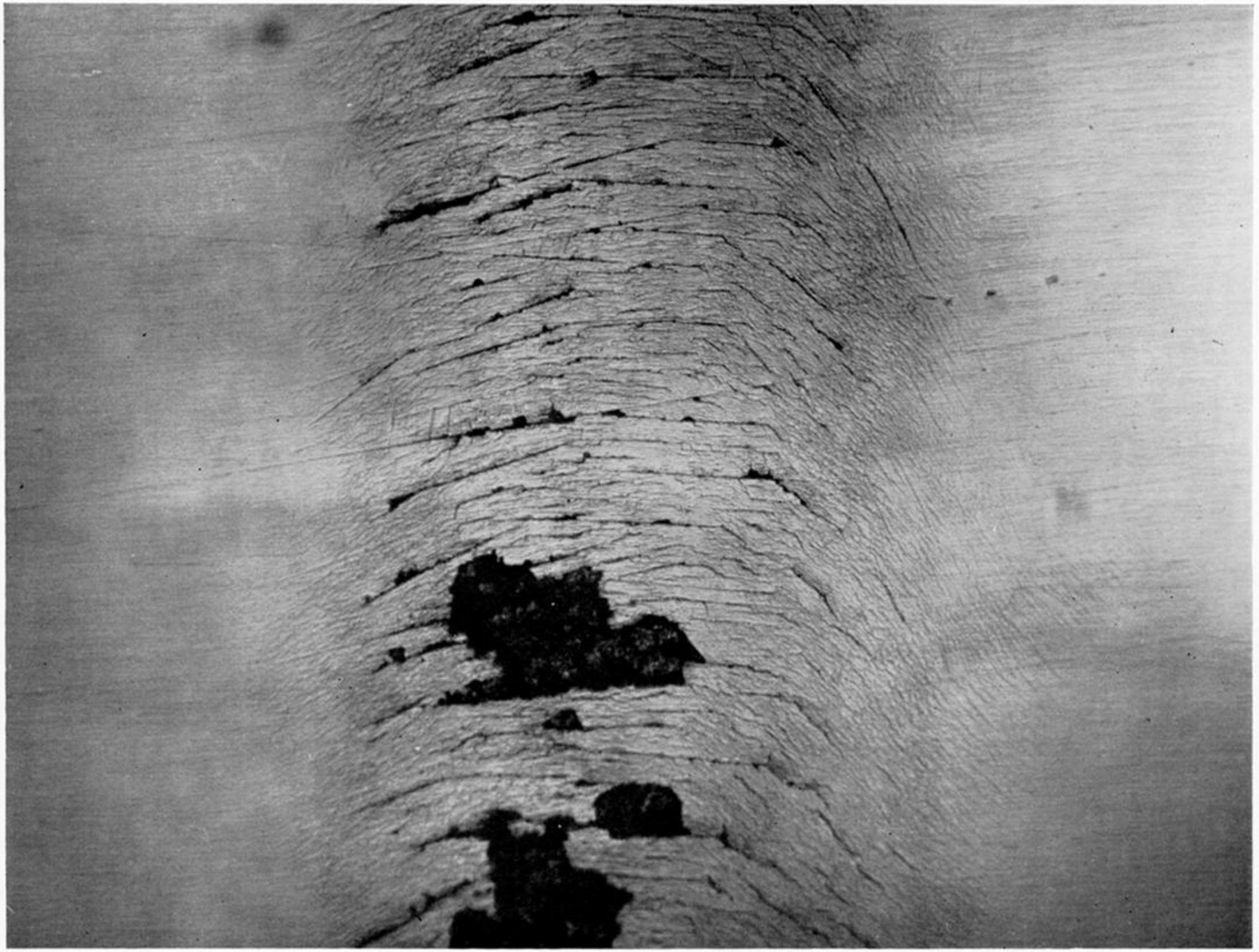

FIGURE 10. Fractures in a polymethylmethacrylate specimen eroded such that the impact surface was tilted at an angle of 9° to the jet axis. The area shown in the lower half of the photograph struck the jet first. (Magn. × 33.)

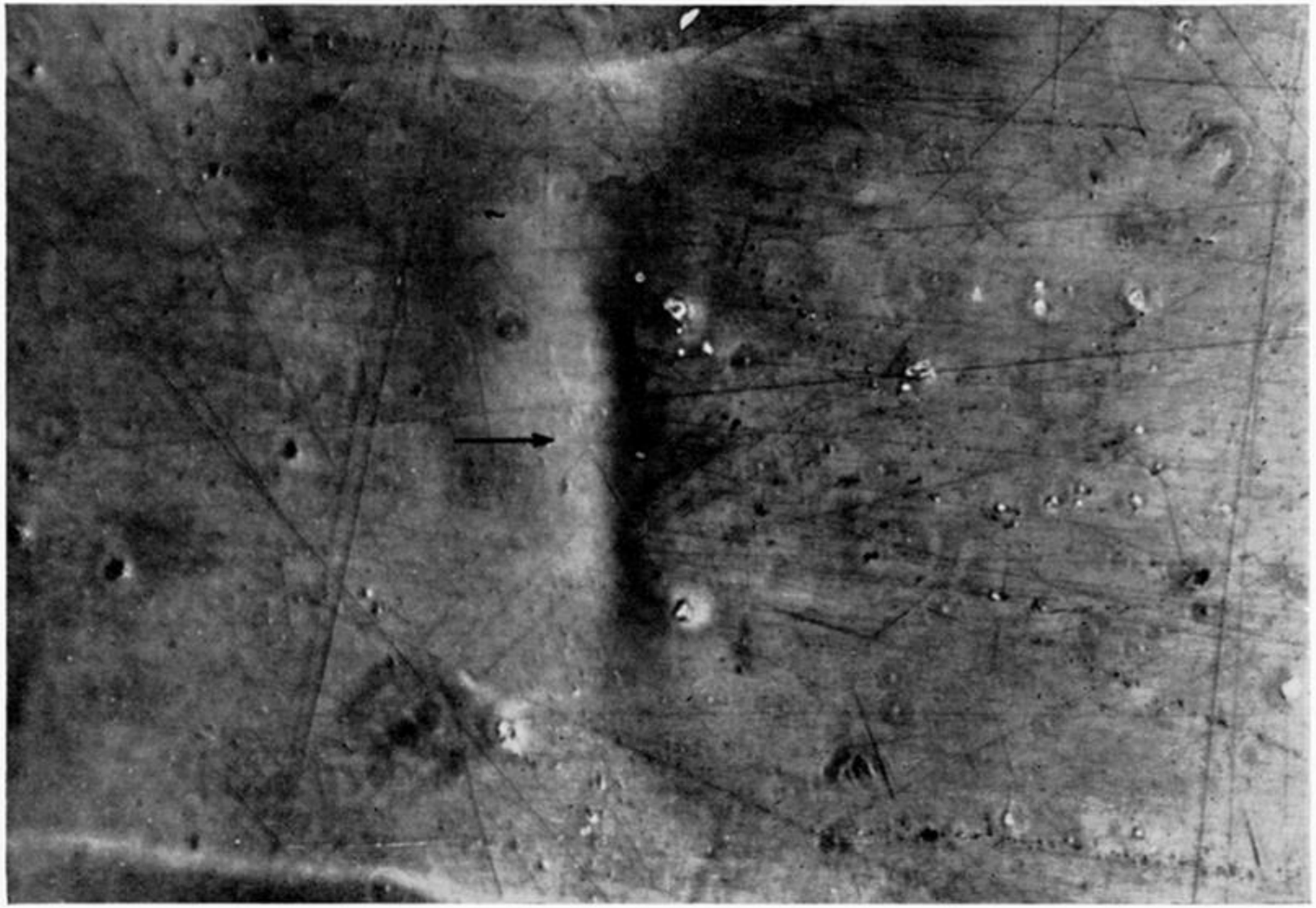

FIGURE 14. A small depression in copper. Depressions similar to this provide the first detectable signs of permanent deformation. The specimen illustrated has received 8000 impacts at 51 m/s. (Magn. × 500.) Phase contrast photograph.

5160

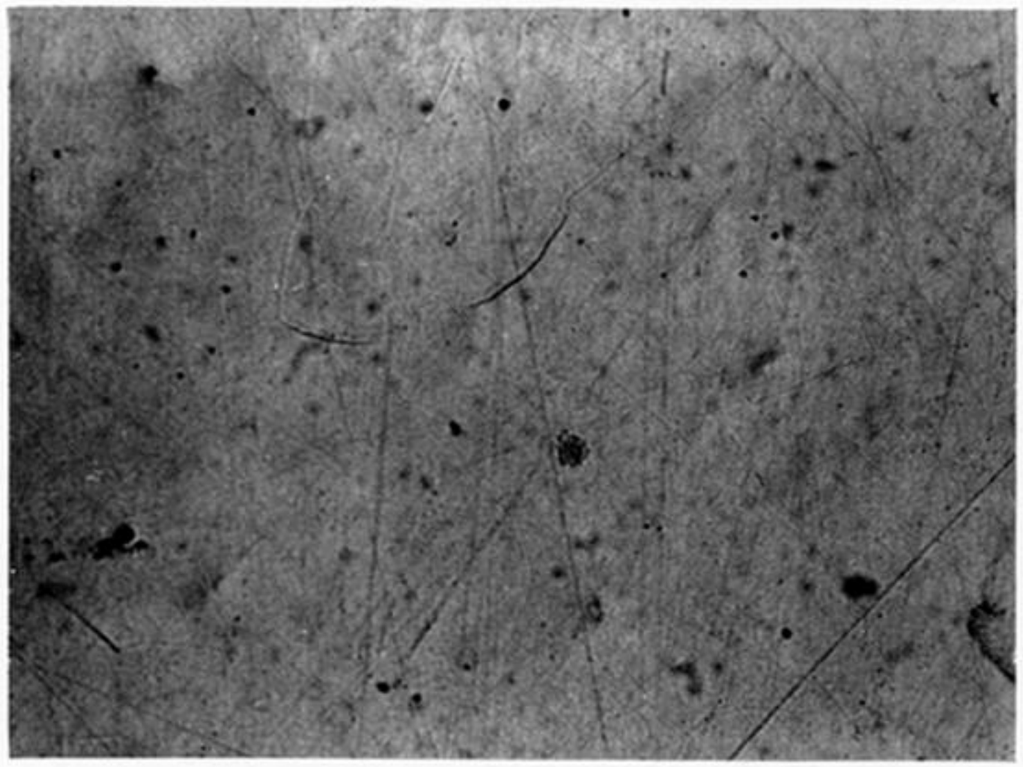

10320

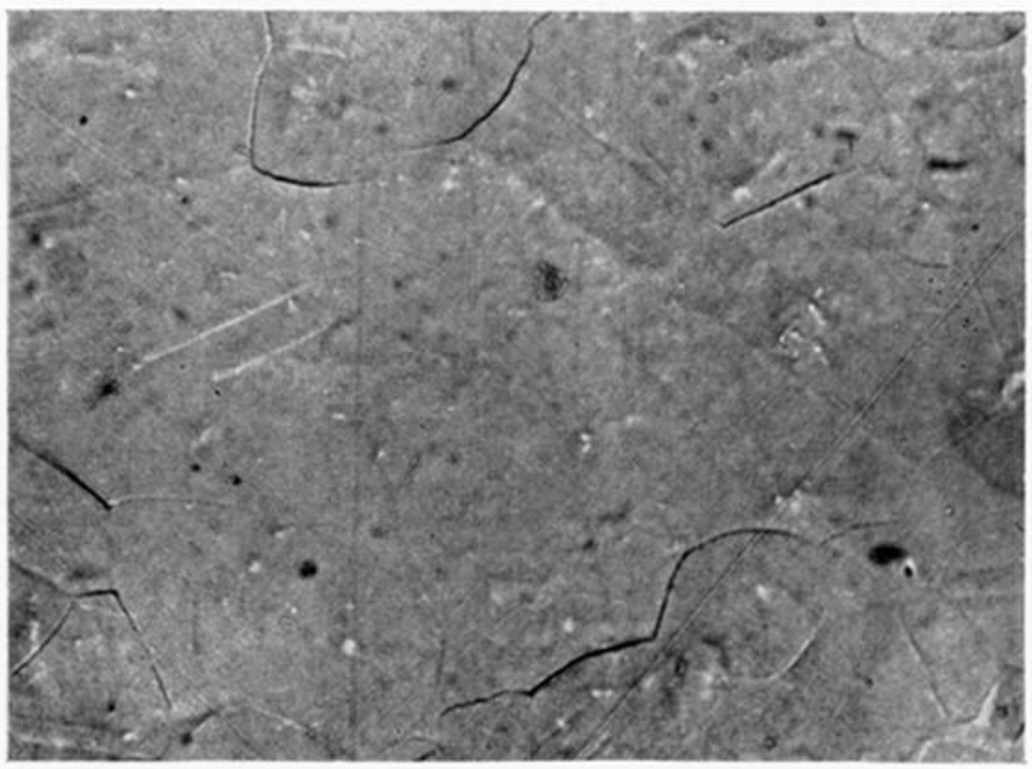

51600

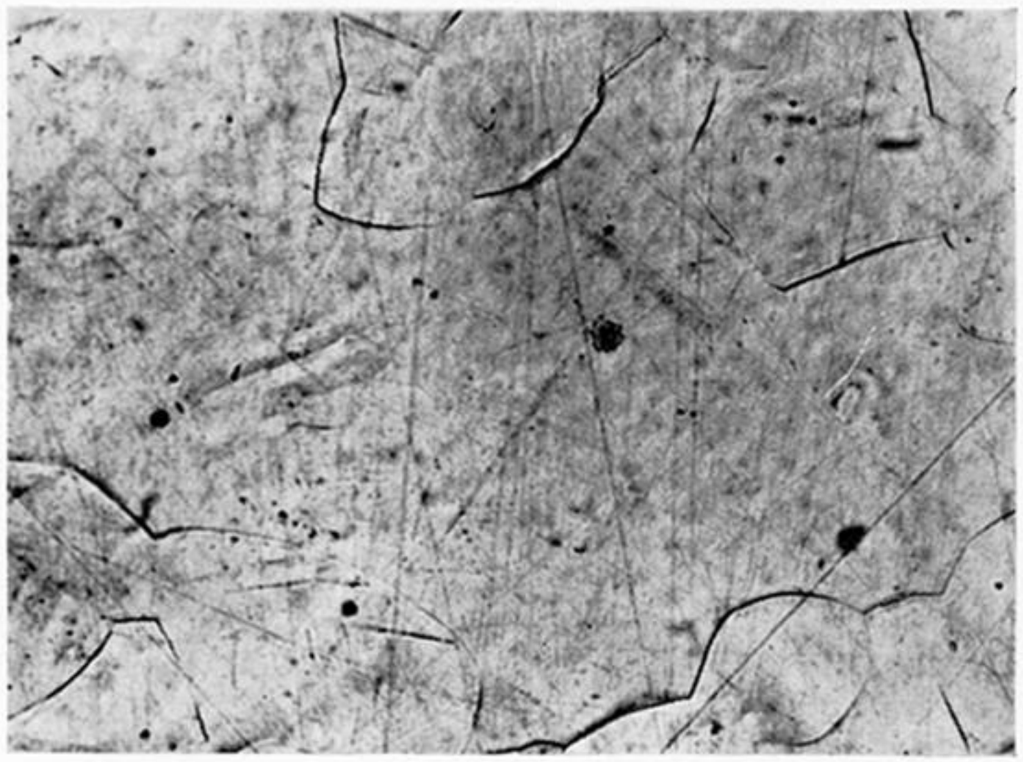

181000

413000

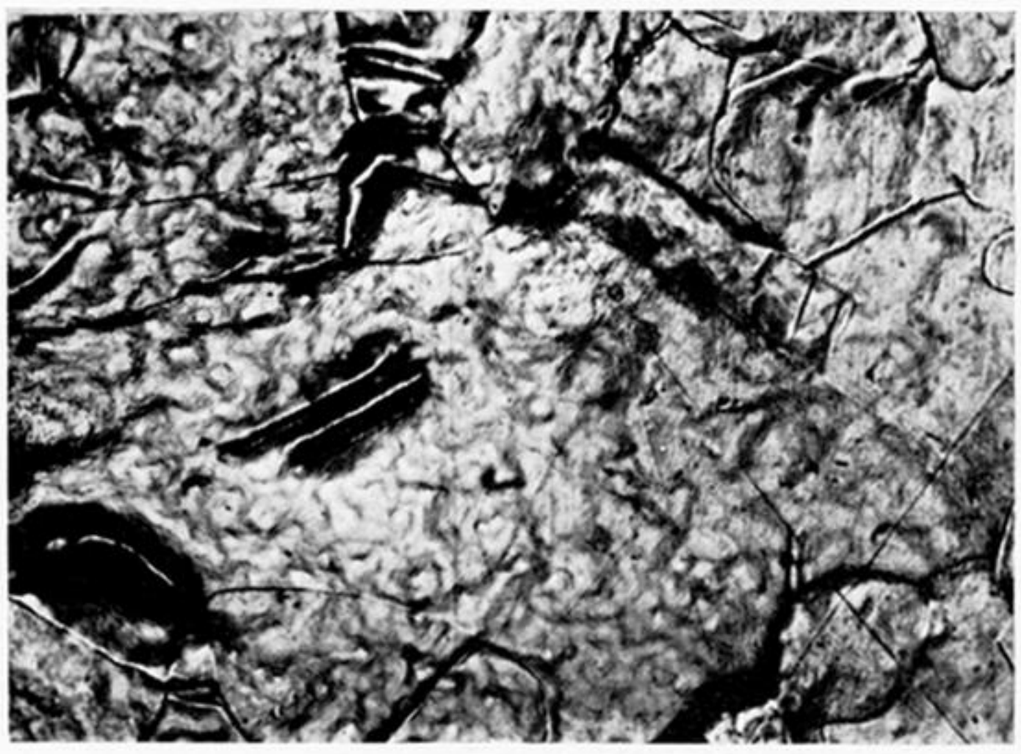

620000

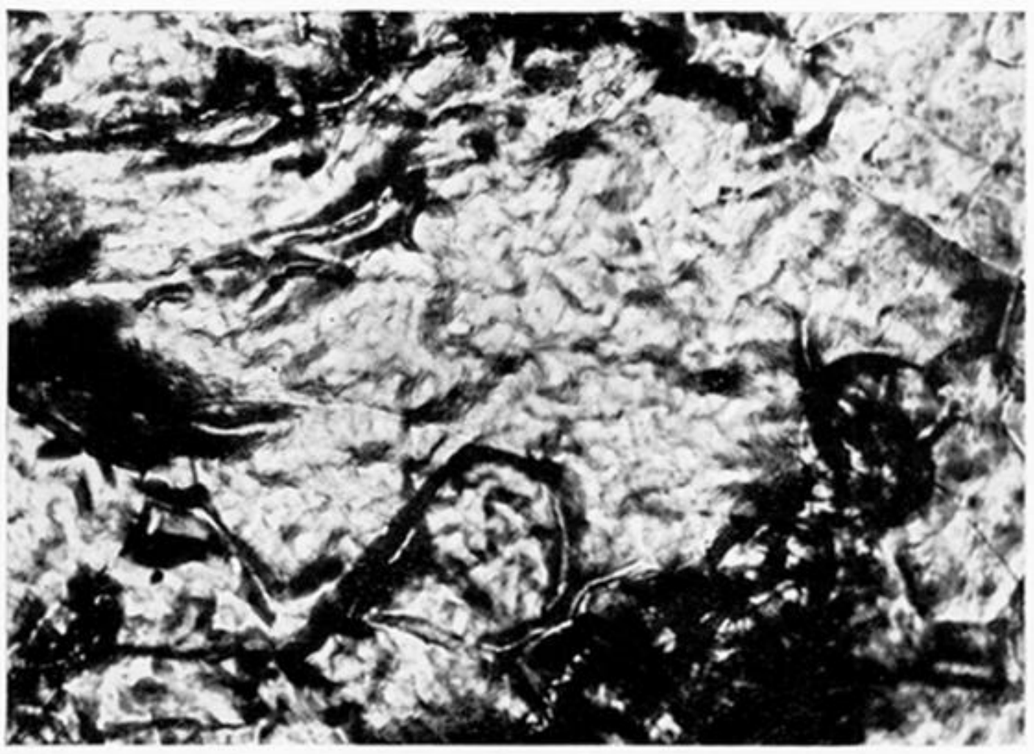

FIGURE 15. The development of erosion damage in copper. The number of impacts is shown besides each frame. The impact velocity was 52 m/s and the water jet diameter 1·35 mm. (Magn. × 190.)

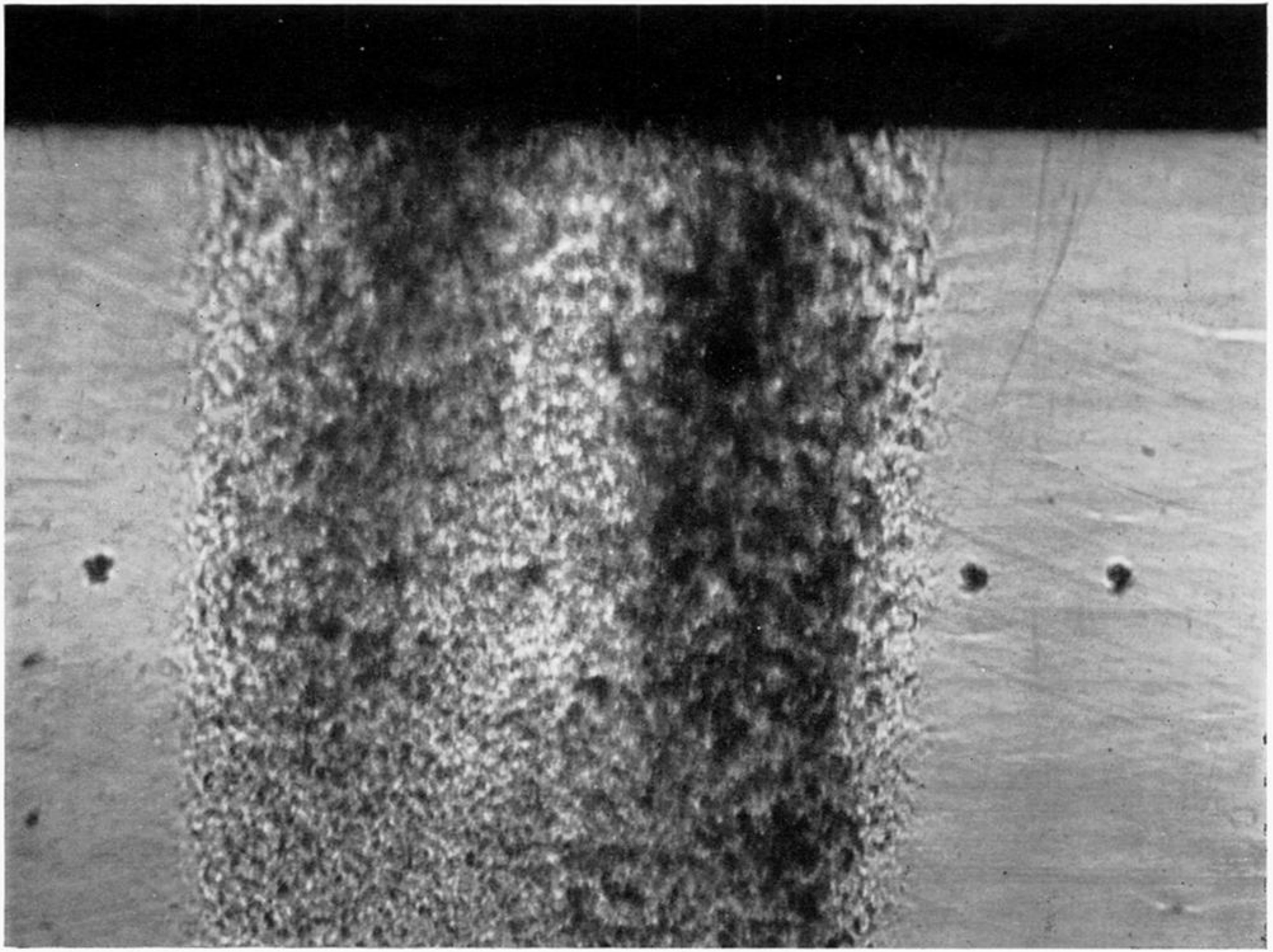

FIGURE 19. Two bands of deformation in a specimen of low carbon steel. The bands run parallel to and lie on either side of the centre line of impact. (Magn. $\times 35$.)

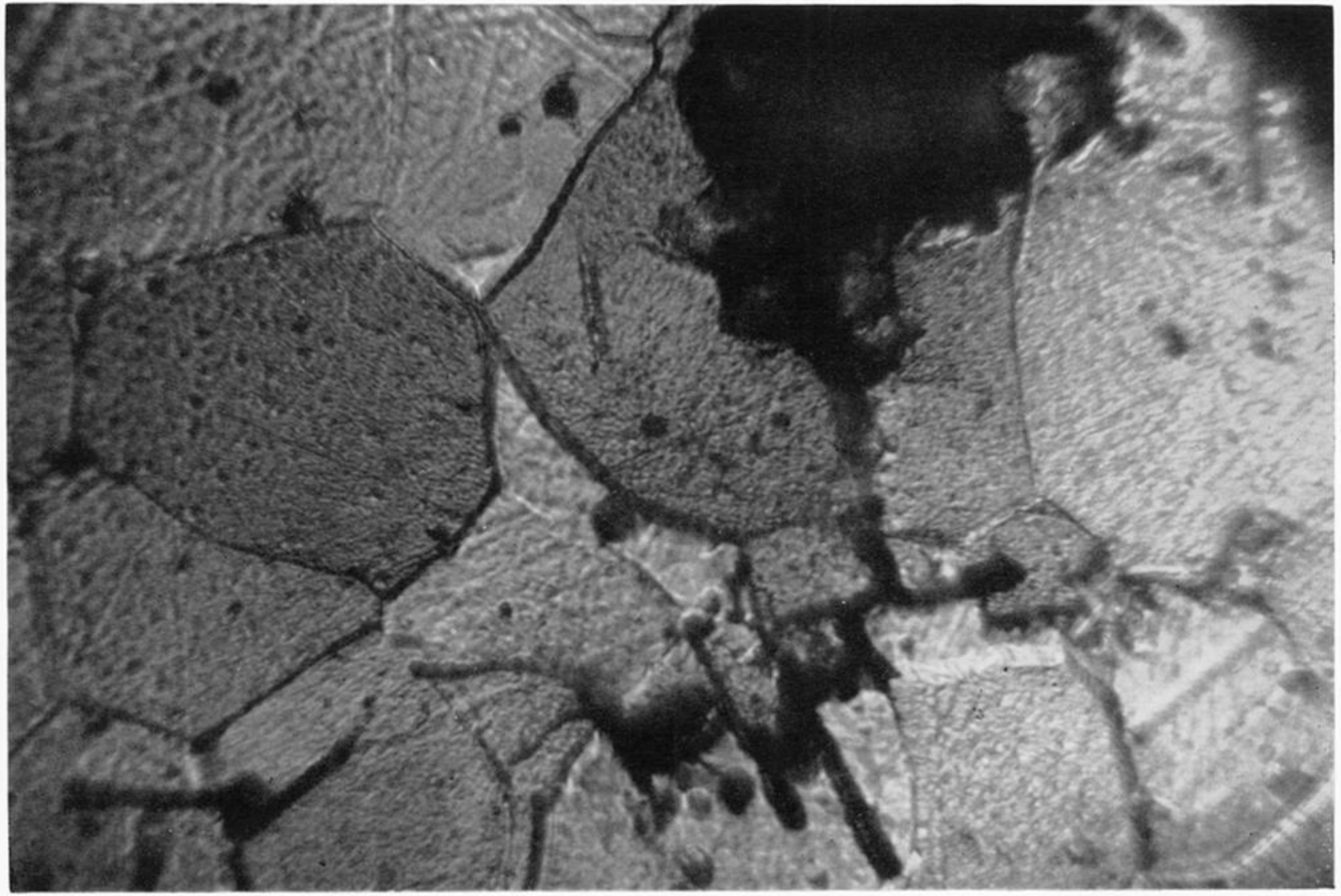

FIGURE 20. A crack spreading from the root of a surface pit in an eroded, sectioned and etched specimen of low carbon steel. 10^6 impacts at 90 m/s. (Magn. $\times 900$.)

FIGURE 21. Shear deformation along twin boundaries in an iron single crystal. The centre of impact was to the right of the area photographed. $2{\cdot}8 \times 10^5$ impacts at 85 m/s. (Magn. $\times 470$.)

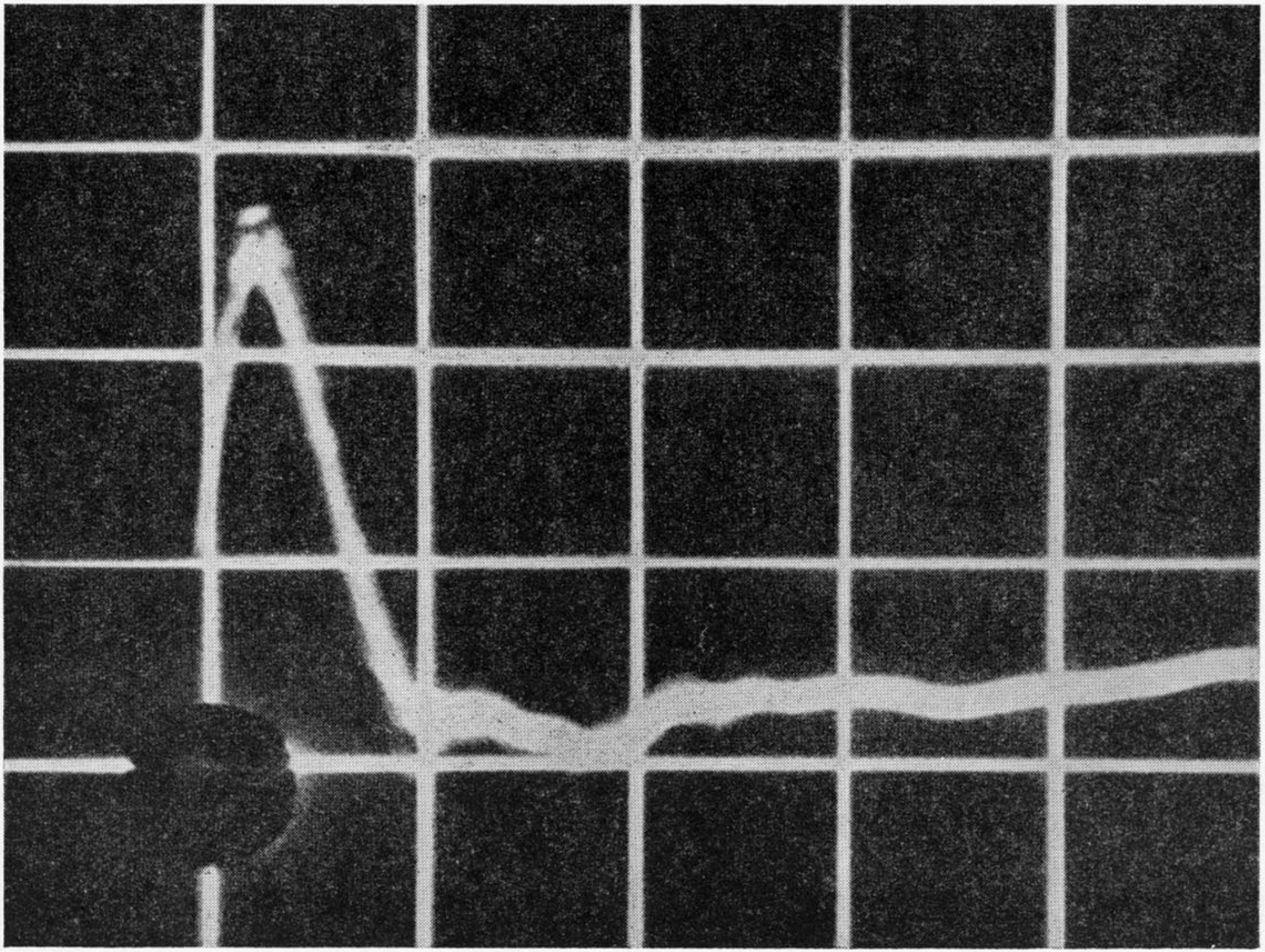

FIGURE 6. A load–time trace for a liquid impact at a velocity of 61 m/s and a water jet diameter of 1·3 mm. One vertical division = 14 Kg. One horizontal division = 5 μs.